

## ABSTRACT

Title of Thesis:       CHARACTERIZING CIGARETTE LIGHTER FLAMES TO  
                              REDUCE UNWANTED IGNITION

Justin Wade Williamson, Master of Sciences, 2003

Thesis Directed By:  Professor André W. Marshall  
                              Department of Fire Protection Engineering

This investigation provides detailed measurements and analysis for improved understanding of ignition from the ‘small’ flames produced by cigarette lighters. This research program is motivated by the need to improve the fire safety of cigarette lighters in response to the juvenile firesetter problem. A novel cigarette lighter concept for improved ignition safety has been developed, characterized, and compared with conventional lighters. Diagnostics were performed to measure laminar near-field plume behavior and turbulent far-field behavior in these small-scale (75W) flames. Plume diagnostics include centerline temperature, heat flux to a horizontal flat plate, and ignition of filter paper. Data was scaled and compared to plume theory

and measurements. Other practical cigarette lighter performance related properties were also noted, such as lighter surface temperatures and cigarette ignition effectiveness.

CHARACTERIZING CIGARETTE LIGHTER FLAMES TO  
REDUCE UNWANTED IGNITION

by

Justin Wade Williamson

Thesis submitted to the Faculty of the Graduate School of the  
University of Maryland, College Park in partial fulfillment  
of the requirements for the degree  
Master of Science  
2003

Advisory Committee:

Professor André W. Marshall, Chair  
Professor James G. Quintiere  
Professor Arnaud Trouvé

©Copyright by

Justin Wade Williamson

2003

## **Acknowledgments**

First I would like to thank Mr. Frank McGarry of the National Association of State Fire Marshals (NASFM) for providing funding for this study and for motivating me to produce results. I would also like to thank Ms Marjorie Armacost for her constructive criticism and complete support concerning the completion of this study. I would also like to thank all of the members of the Fire Flow research group and all of the students from the Fire Engineering and Thermal Sciences Laboratory. They have provided me with a friendly and supportive working environment, as well as plenty of constructive feedback and suggestions. I would also like to thank Mr. Steve Hill of the Bureau of Alcohol, Tobacco, and Firearms (ATF) for the use of equipment critical to the success of this research. I also wish to acknowledge Professor Jim Qunitiere for his useful suggestions and productive discussions. Finally, I would like to thank Professor André W. Marshall for his infinite patience and willingness to assist in any way possible with the success of this project.

## Table of Contents

List of Tables.....	v
List of Figures .....	vi
Chapter 1: Introduction .....	1
1.1 Overview .....	1
1.2 Literature Review .....	2
1.3 Objectives.....	9
Chapter 2: Experimental Approach.....	11
2.1 General Methodology.....	11
2.1.1 Nozzle Designations.....	11
2.1.1.1 Diffusion Lighter.....	11
2.1.1.2 Premixed1 Lighter.....	14
2.1.1.3 Premixed2 Lighter.....	16
2.1.1.4 Prototype Lighter.....	18
2.1.2 Key Operation Parameters .....	22
2.2 Experimental Apparatus.....	23
2.2.1 Flow Calibration.....	25
2.2.2 Stability and Alignment .....	26
2.3 Diagnostics .....	26
2.3.1 Temperature and Transition to Turbulence.....	27
2.3.2 Heat Flux to a Horizontal Flat Plate.....	29
2.3.3 Ignition of Filter Paper .....	32
2.4 Summary .....	34
Chapter 3: Results .....	35
3.1 Characterizing Existing Cigarette Lighters .....	35
3.1.1 Flame Height.....	35
3.1.2 Temperature .....	36
3.1.3 Heat Flux .....	42
3.1.4 Unwanted Ignition.....	48
3.2 Development and Characterization of Prototype .....	51
3.2.1 Prototype Flame Height .....	53
3.2.2 Prototype Temperature.....	53
3.2.3 Prototype Surface Temperature.....	57
3.2.4 Prototype Heat Flux .....	59
3.2.5 Prototype Unwanted Ignition .....	63
Chapter 4: Conclusions .....	64
4.1 Temperature Measurements .....	64
4.2 Heat Flux Measurements.....	65
4.3 Ignition of Filter Paper Measurements.....	66
4.4 Overall Prototype Performance.....	67

Appendix A: Illustration of Fuel Orifice.....	69
Appendix B: Proposed Cigarette Lighter Design Utilizing the Prototype Concept.....	70
Appendix C: Illustration of the National Instruments Program Diagram used for High Frequency Temperature Measurements .....	71
Appendix D: Matlab Program for Processing Heat Flux to a Horizontal Flat Plate.....	73
Appendix E: Prototype Surface Temperature Prediction Method.....	77
Bibliography.....	81

## **List of Tables**

1.	Key nozzle physical characteristics.....	21
2.	Existing cigarette lighter hazard characteristics.....	54
3.	Hazard characteristics for all nozzles tested .....	68

## List of Figures

1.	Number of fires started by juveniles, Rochester Fire Department, 1985-1993....	3
2.	Percentage of fires started by juveniles resulting in structural damage, injury or death, Rochester Fire Department, 1985-1993.....	3
3.	Percentage of juvenile fires started by matches and lighters, Rochester Fire Department, 1985-1993.....	4
4.	Scale drawing of a commercial Diffusion Cigarette Lighter .....	13
5.	Scale drawing of a commercial Premixed1 Cigarette Lighter .....	15
6.	Scale drawing of a commercial Premixed2 Cigarette Lighter .....	17
7.	Scale drawing of the Prototype cigarette nozzle .....	20
8.	Nozzles with images of visible flames.....	21
9.	Experimental setup.....	24
10.	Illustration of one side of the water-cooled clamp.....	24
11.	Flow calibration data.....	25
12.	Thermocouple probe design.....	29
13.	Water-cooling device for the prototype nozzle.....	30
14.	Illustration of the radial energy balance of the copper plate .....	32
15.	Sample IR image with associated best-fit temperature profile .....	33
16.	Centerline temperature profiles for the three existing cigarette lighter nozzle designs.....	37
17.	Scaling analysis of centerline temperature data compared to data from McCaffrey .....	39
18.	Scaling analysis of temperature fluctuations.....	42
19.	Premixed1 surface temperature performance for 110 s of operation without the water-cooling clamp.....	43

20.	Heat flux profiles corresponding to the maximum observed incident heat flux .....	44
21.	Stagnation point heat fluxes as a function of height .....	44
22.	Scaling analysis of stagnation point heat flux assuming laminar flow and laminar stagnation point theory.....	47
23.	Sample plume shadowgraphs .....	48
24.	Ignition data for the three existing nozzles .....	49
25.	Ignition data versus stagnation point heat flux data.....	50
26.	Scaling of ignition data .....	50
27.	Centerline temperatures of all tested nozzles.....	55
28.	Scaling analysis of all tested nozzles compared to data taken by McCaffrey....	56
29.	Temperature fluctuations of all tested nozzles.....	56
30.	Legend for Figures 30 to 32 .....	60
31.	Tube 1 (inner tube) surface temperatures.....	60
32.	Tube 2 (middle tube) surface temperatures.....	61
33.	Tube 3 (outer tube) surface temperatures.....	61
34.	Radial heat flux profiles corresponding to the peak observed stagnation point heat flux for all nozzles .....	62
35.	Stagnation point heat fluxes versus height for all nozzles tested.....	62

# Chapter 1: Introduction

## 1.1 Overview

Small flames, such as those found in candles, matches, cigarette/utility lighters, and the incipient fire pose a significant fire hazard. These small flames can release enough thermal energy to cause unwanted ignition and sustain burning. This investigation focuses on the ignition hazard from small cigarette lighter flames. Small ignition sources are dangerous and can produce a small fire that can go unnoticed for a long period of time. Of these small sources, candles are most commonly recognized as fire hazards. The National Fire Protection Association (NFPA) recognizes this risk and has published a fact sheet with safety tips for using candles in the home.<sup>1</sup> Other small ignition sources include matches and cigarette lighters. The NFPA also recognizes the risk from these sources in Hall's publication, *Children Playing with Fire*.<sup>2</sup> Cigarette lighter flames produce a high risk of ignition and also an opportunity for modification, and therefore need special consideration.

Recent efforts for improving lighter safety have centered on developing mechanical child safety features.<sup>3</sup> However, these child safety features do not reduce the unwanted ignition propensity of the *lighter flame*. There is a need for detailed flame characterization of cigarette lighters in order to determine the ignition propensity of these devices and to develop methods for reducing ignition propensity. The current standard for improving safety focuses on adding mechanical child safety features.<sup>4</sup> These additional mechanical child safety features do nothing to resolve the unwanted ignition propensity of the lighter flame. This research focuses on

characterizing and modifying the driving force of ignition, the flame, and illustrates methods that reduce the ignition hazard from that source.

The cigarette lighter safety problem is particularly interesting. Existing mechanical safety features are cumbersome and are often bypassed by the user in order to improve ease of use. These “child safety” features are intended to inhibit use of the lighter by persons who lack the motor skills and understanding to operate the lighter. Studies conducted by the National Association of State Fire Marshals (NASFM), such as the Juvenile Firesetter Program, have shown that these features are insufficient for reducing unwanted ignition by juveniles ages 4 to 16 as shown in Figures 1 to 3.<sup>3</sup> Also, the American Society for Testing and Materials (ASTM) standard for regulation of cigarette lighters, ASTM F400-00, is qualitative in nature with respect to unwanted ignition propensity and does not characterize the increased hazard of many new cigarette lighter designs.<sup>4</sup> The NASFM recognizes that there is a need for detailed thermal characterization of cigarette lighters in order to determine the ignition propensity and methods for reducing the ignition propensity.

## **1.2 Literature Review**

There is very little previous work characterizing the ignition hazard from cigarette lighters. However, previous work on the thermal behavior of fire plumes may be applied to cigarette lighters with appropriate scaling. Many studies have characterized the gas temperature above a fire source, heat transfer to surfaces above a fire source, ignition of materials with external heating, and transition to turbulence in plumes.

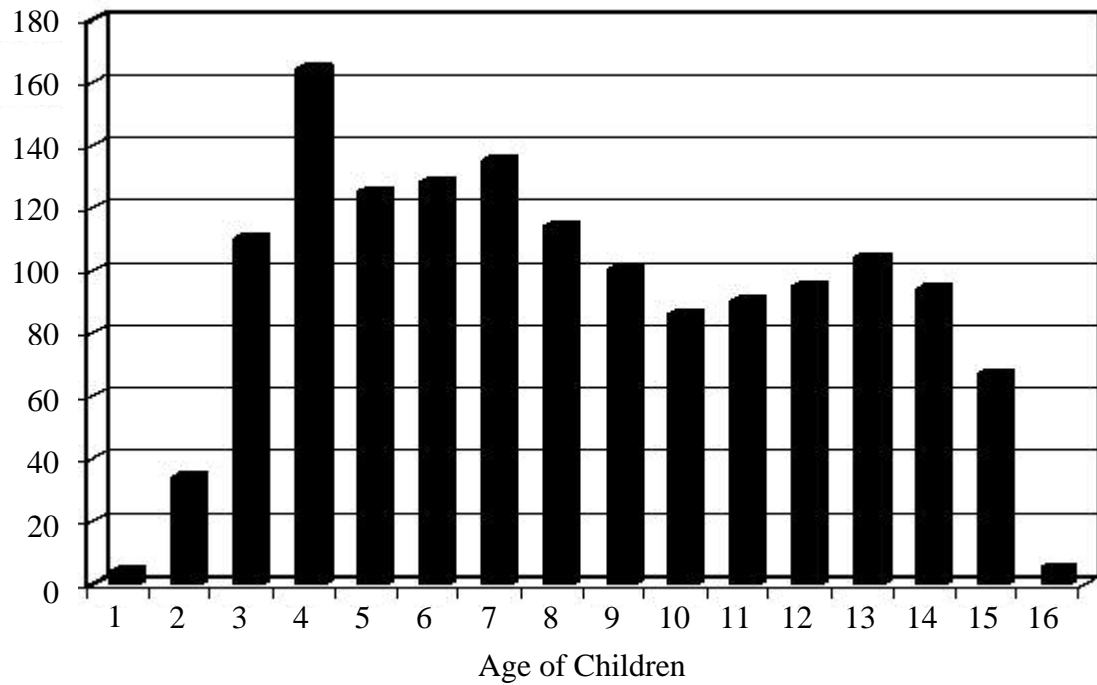


Figure 1: Number of fires started by juveniles, Rochester Fire Department, 1985-1993.<sup>3</sup>

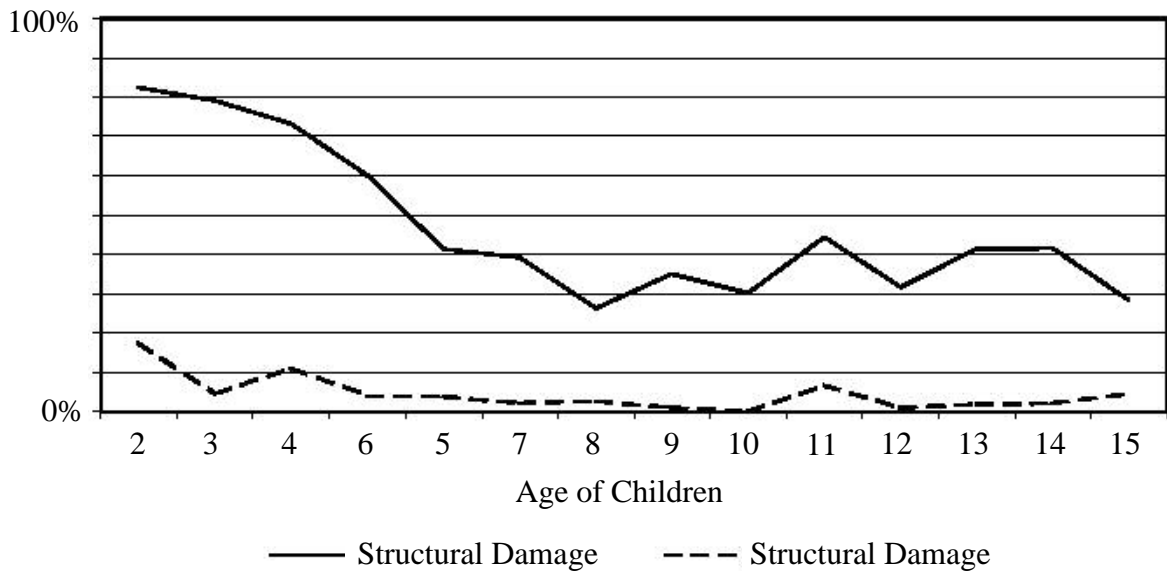


Figure 2: Percentage of fires started by juveniles resulting in structural damage, injury or death, Rochester Fire Department, 1985-1993.<sup>3</sup>

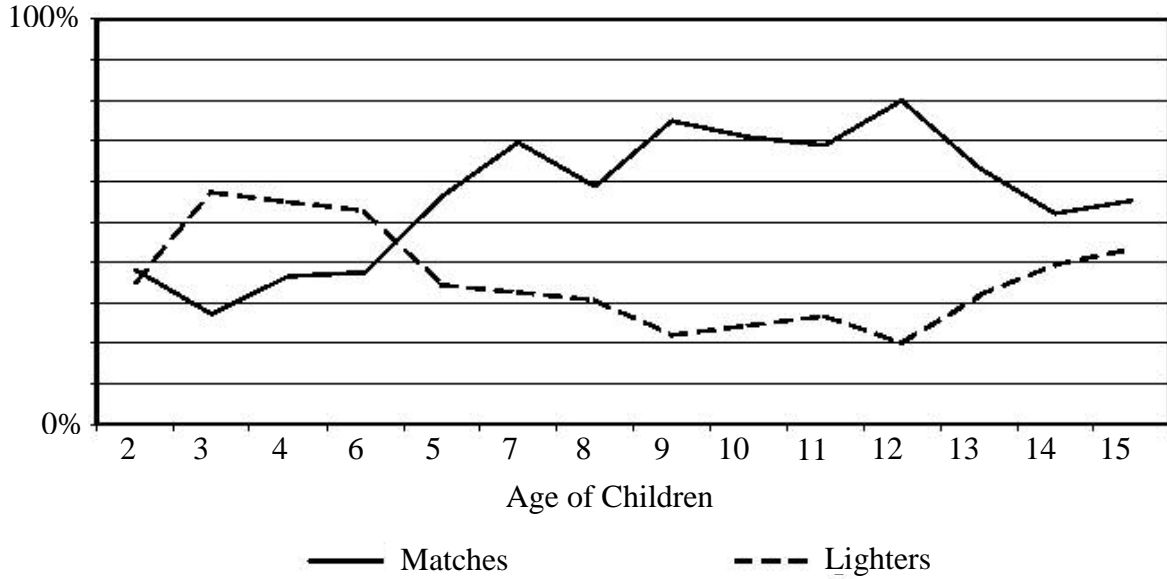


Figure 3: Percentage of juvenile fires started by matches and lighters, Rochester Fire Department, 1985-1993.<sup>3</sup>

Temperature profiles are a key thermal characteristic of fire flows as they are indicative of the heating potential of the flow. Lighter nozzles that produce higher plume temperatures should correspondingly have a higher risk of ignition than those with lower temperatures assuming comparable velocities. Morton et al. previously determined the centerline velocity and temperature distributions in a turbulent plume issuing from a point source.<sup>5</sup> He found that the centerline temperature decay along the plume axis followed a (-5/3) power law:<sup>5</sup>

$$\frac{T - T_{\infty}}{T_{\infty}} = \frac{5\dot{Q}}{6\alpha} \left( \frac{9}{10} \alpha \dot{Q} \right)^{-1/3} z^{-5/3}, \quad (1)$$

where  $T$  is the centerline plume temperature,  $T_{\infty}$  is the ambient temperature,  $\dot{Q}$  is the energy release rate of the flame,  $\alpha$  is the plume entrainment coefficient constant experimentally found to be 0.11, and  $z$  is the characteristic height above the source, based on integral analysis of the turbulent plume equations. McCaffrey measured the

centerline temperature decay along the plume axis above fire sources.<sup>6</sup> He found that the temperature decayed according to the same theoretical power law in the plume zone sufficiently far from the source. He also identified a flame zone with constant temperature and an intermittent zone where the temperature decayed inversely with position along the plume axis. Flows from cigarette lighter flames are rarely turbulent near the source; therefore it is important to observe the laminar characteristics and compare them to classical laminar theories for appropriate analysis. The laminar plume equations were solved by Fujii using similarity analysis.<sup>7</sup> His laminar analysis predicted that centerline temperatures should decay inversely with position above the plume. The flow generated by cigarette lighters can be considered a forced flow, especially in cases where the fuel is premixed with air. Morton has investigated plumes generated by a steady release of mass, momentum and buoyancy, analytically illustrating the difference between forced plumes and purely buoyant plumes. The results of his analysis show that forced plumes decay similarly to a jet in the near field with (-1) power law decay, transitioning to plume decay in the far field with an offset.<sup>7</sup>

Transition to turbulence has been studied extensively for vertical plumes. Determining if and where this turbulence occurs is of great importance to scaling data in the flows produced by cigarette lighter flames because the flow is initially laminar, eventually transitioning to turbulence. Krishnamurthy et al. and Jiang et al. have studied buoyant flows adjacent to a vertical surface using experimental and modeling approaches respectively.<sup>21,22</sup> This geometry is of particular interest for convective heating of the side wall, as the convective heating coefficient has a strong dependence

on the level of turbulence. Bejan and Kimura et al. have studied free buoyant plumes, and provide a fundamental method for determining the transition to turbulence.<sup>23,24</sup>

Using the instability analysis prescribed by Kimura et al., a predictor of the transition to turbulence can be predicted by  $z_t \sim Q^{-1/2}$ , where  $z_t$  is the turbulent transition height and  $Q$  is the energy release rate of the flame.<sup>24</sup> Similarly, a critical Rayleigh number approach,

$$\text{Ra}_q = \frac{gz_{tr}^2 \dot{Q}}{(\alpha \nu k)_{air} T_\infty} \leq 10^{10}, \quad (2)$$

where  $g$  is the gravitational constant,  $z_{tr}$  is the height for transition to turbulence, and  $(\alpha \nu k)_{air}$  are the thermal diffusivity, kinematic viscosity, and conductivity of air respectively, can be used as described by Bejan.<sup>23</sup>

Heat transfer to horizontal surfaces above large fire sources has also been studied extensively. This configuration has been used for studying heat loading on ceilings and other objects above fires. Heat transfer to the horizontal surface results from plume impingement and the formation of a wall jet traveling radially outward below the horizontal surface. In this study, this heat flux was used as a metric for ignition propensity of the source. Alpert determined an analytical solution from integral analysis for ceiling jet temperatures, velocities, and jet thicknesses.<sup>9</sup> He was able to determine a local heat flux to the ceiling from the theory that he developed for ceiling jets. He found a dimensionless heat flux:

$$\xi = q'' H^2 / \dot{Q}, \quad (3)$$

where  $q''$  is the incident heat flux, and  $H$  is the ceiling height, from his turbulent heat transfer analysis.<sup>9</sup> Veldman et al. and Faeth et al. conducted experiments for ceiling

jet heat transfer.<sup>10,11</sup> They found significant scatter in the heat flux data with only limited agreement with the Alpert's ceiling jet theory. They attributed the scatter to other phenomena that may be important to the ceiling heat transfer including radiation effects. Chow and Motevalli have performed numerical studies of the ceiling jet to characterize the velocity and temperature profile of the flow as a function of the radius.<sup>12,13</sup> These profiles are useful for calculating heat flux to the ceiling surface, however, the studies do not evaluate the steady state solution for a thermally thin ceiling. The thermally thin ceiling case is of great importance to the technique used in this study because the temperature of the surface was determined by Infra Red imaging of the back-side of the ceiling at the steady state condition. This is discussed in detail in 2.3.2. Motevalli et al. has investigated the small scale steady state case. His study illustrates that there is negligible difference between the transient and the steady state ceiling jet flow; however, it does not characterize heat transfer to the ceiling.<sup>14</sup> This study will develop a method to calculate total heat transfer to the ceiling without characterizing the fluid flow.

The ability of a cigarette lighter to ignite thin materials is of particular interest in determining the devices safety performance. This study focuses on the ignition of thermally thin flat materials oriented in the horizontal 'ceiling' configuration. Unfortunately, much of the ignition research conducted is focused on the thermally thick or semi-infinite solid assumption. Relatively little work has been done with thermally thin solids. This configuration is identical to the heat flux measurement configuration and the heat flux results are directly correlated with the ignition tests. This comparison will help to determine if the heat flux measurements alone are in fact

indicative of ignition propensity. Drysdale has discussed the theory behind ignition of thermally thin slabs based on the solution of the differential one-dimensional heat conduction equation, showing that regardless of the mode of heat transfer, ignition time is directly proportional to the thermal capacity per unit area ( $\tau\rho c$ ) where  $\tau$  is the thickness,  $\rho$  is the density and  $c$  is the specific heat of the ignition material.<sup>15</sup> Studies performed by Zhou et al., Thomson et al., Atreya et al., and Moghtaderi et al. discuss methods for determining critical heat fluxes and temperatures for ignition of various materials under several different heating conditions. These studies used piloted ignition and thermally thick materials.<sup>16,17,18,19</sup> However, the energy balance method used is quite similar to the method used in the current investigation for thermally thin solids:

$$q'' = \tau\rho c \frac{\partial\theta}{\partial t} + h_c\theta, \quad (4)$$

where  $h_c$  is the convective cooling rate of the far side due to natural convection, and  $\theta = T_{ig} - T_\infty$  such that  $T_{ig}$  is the ignition temperature of the solid.<sup>15</sup> Nelson et al. performed a study of thermally thin solids in the cone calorimeter illustrating that the critical heat flux can be determined graphically by from  $1/t_{ig}$  versus the incident heat flux,  $\dot{q}''$ , where  $t_{ig}$  is the time to ignition.<sup>20</sup> We will use a similar technique in this study using cigarette lighter flames as the heat source. Ignition testing of different cigarette lighters will illustrate that each lighter has the propensity to ignite a specific material within a region of the plume where the energy transfer is sufficient, and it will illustrate that modifications can be made to the nozzle geometry that can reduce this region of ignition.

### 1.3 Objectives

The objectives of this study are to characterize ignition propensity of cigarette lighters, and to create a concept that will demonstrate an improvement in unwanted ignition propensity from a cigarette lighter without adding mechanical child safety features. A method was developed to characterize the ignition propensity of cigarette lighters. The ignition propensity of three existing cigarette lighters were characterized using this methodology, followed by an evaluation of one prototype design using the same methodology. Three characteristic parameters that describe ignition propensity were evaluated:

- centerline temperature profiles while noting transition to turbulence,
- heat flux profiles to a horizontal flat plate ,
- and ignition of filter paper.

Each of these characteristics was determined experimentally such that a comparison of the unwanted ignition propensity of the three existing designs and the prototype design can be made.

The prototype design was fabricated based on characteristics of the three existing lighters. Some of the characteristics of the three existing lighters demonstrate improved unwanted ignition propensity or a need for improvement. These characteristics were observed, and then utilized in the prototype concept. There is a large opportunity for modification of cigarette lighters because they can be designed based on simple geometry and the low ignition energy requirements of cigarettes. These properties allow for a simple design that will provide local heating to the cigarette and reduced heating to other objects. A simple flame recession was

introduced to achieve this. The recession was designed according to the geometry of the cigarette such that only objects of similar geometry or objects smaller than a cigarette could be inserted into the recession. The recession acts as a medium to absorb energy from the flame while increasing the distance between the flame source and the exit of the hot gasses. Compared to an open flame, this prototype has a hidden flame that is less enticing to curious children, and has significantly improved exit gas properties. Design modifications will be discussed in more detail in the approach section. The prototype lighter characterization measurements demonstrated that unwanted ignition propensity could be improved without the addition of mechanical child safety features.

## **Chapter 2: Experimental Approach**

### **2.1 General Methodology**

In order to create a set of controlled experiments that would accurately and consistently compare different cigarette lighter designs, important operation parameters were determined and a system was created that could control those parameters for every case. The methodology for testing was based on characterizing different types of cigarette lighter nozzles. The experiment was designed in order to keep certain parameters constant while evaluating the effects of varying nozzles on ignition propensity.

#### **2.1.1 Lighter Nozzle Designations**

Changes in flame behavior were evaluated while varying the nozzle type and or burner geometry. All data are illustrated using the designations listed below. Using this methodology, flow structures, heat fluxes, plume centerline temperatures and ignition propensity were measured for each flame configuration. The configurations are designated as Diffusion, Premixed1, Premixed2 and Prototype depending on the burner type. Illustrations of these lighters are provided in Figures 4-7.

##### **2.1.1.1 Diffusion Lighter**

For the Diffusion lighter, a standard port-type nozzle is used to produce a candle like flame that is widely recognized. Cigarette lighters with port-type nozzles can be easily obtained from any store where cigarettes are purchased. A scale

drawing detailing the fuel system of the commercial design is illustrated in Figure 4. In this case, the fuel is directly injected through a 0.5 mm diameter opening into the ambient air where it begins to mix diffusely. The fuel is ignited using a spark that allows for steady, sustained burning of the fuel. The reaction zone only occurs at the fuel-air interface as determined by diffusion. The orange/yellow color as seen in Figure 8 is attributed to heated carbon particles in the flow formed by decomposition, or pyrolysis, of the fuel prior to burning. For testing of this nozzle, the fuel pathway was modified slightly from its original configuration. In the commercial design, the default fuel pathway is closed by a simple plug, as labeled in Figure 4, forced closed by a spring. Removal of the plug made the default pathway open without significantly changing the fuel injector geometry. The heat shield was also removed for testing purposes because of its weak structural significance and negligible impact on flame behavior. The flame does not exist within the flame shield in the actual design because no air can be entrained through the shield. Therefore, this modification had no impact on the flame behavior. Details of some design characteristics are listed in Table 1.

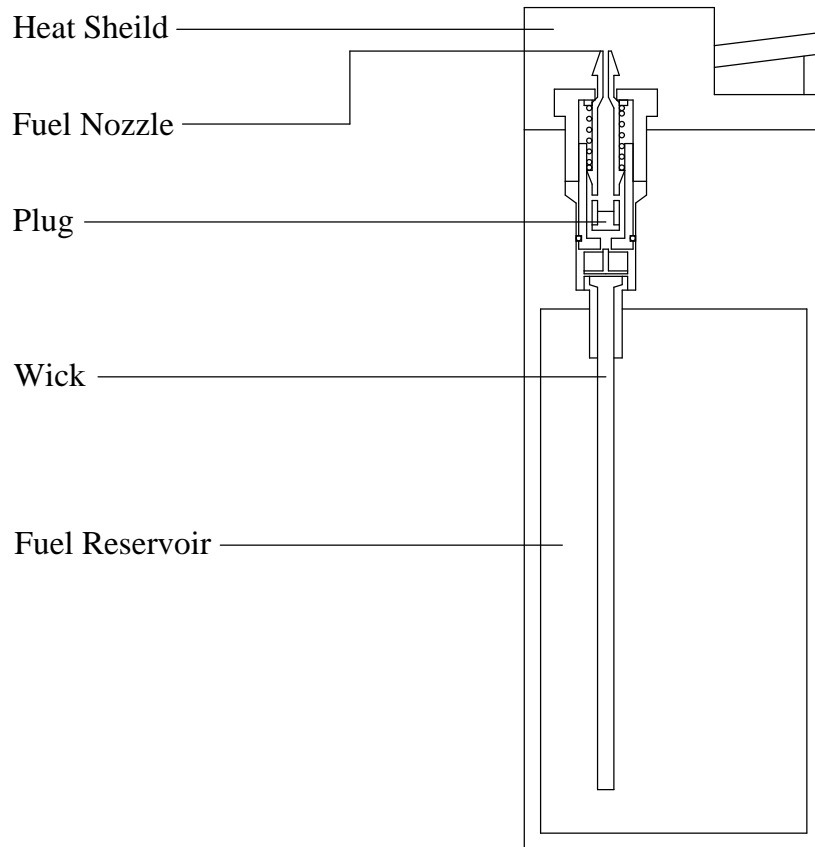


Figure 4: Scale drawing of a commercial Diffusion Cigarette Lighter.

### 2.1.1.2 Premixed1 Lighter

The Premixed1 lighter uses a novelty Bunsen burner type nozzle, which is widely available at specialty stores and online. A scale drawing of the commercial design focusing on the fuel flow system is illustrated in Figure 5. This nozzle produces a blue flame due to fuel air mixing prior to combustion. The fuel is injected through a 70  $\mu\text{m}$  orifice, as shown in Appendix A, to produce a high velocity jet. This jet is injected through a vented chamber where it entrains air prior to combustion. The fuel air mixture is then injected into a small combustion chamber of depth  $\delta_{light} = 6 \text{ mm}$ , where it is ignited by a piezoelectric spark device. A simple wire mesh, or flame stabilizer, encloses the combustion chamber to provide limited stability of the flame in windy conditions. Some of the fuel reacts in this chamber and the remainder of the unburned fuel and air pass through the flame stabilizer prior to its combustion. The mixing nozzle, combustion chamber, and the part of the flame that exists outside of the chamber are illustrated in Figure 8. Since this nozzle produces a combustible fuel air mixture, the reaction zone occurs evenly at all locations in the flame, not only at the outer edge of the flame, but along the centerline as well. This uniform combustion zone produces a blue flame because little soot is formed, reducing its luminosity. Details of some design characteristics are listed in Table 1. No design modifications were made to the burner geometry in the experimental configuration.

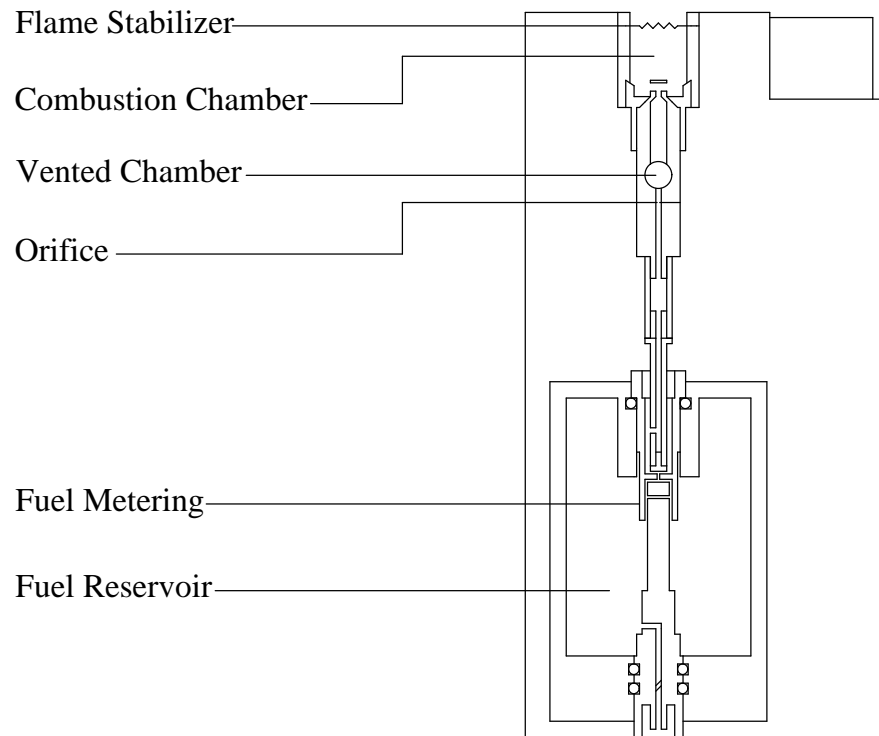


Figure 5: Scale drawing of a commercial Premixed Cigarette Lighter.

### 2.1.1.3 Premixed2 Lighter

The Premixed2 lighter also uses a novelty Bunsen burner type. This lighter is also widely available at specialty stores and online. A scale drawing of the commercial design focusing on the fuel flow system is illustrated in Figure 6. The lighter produces a blue flame due to fuel air mixing prior to combustion. The fuel is injected through a  $70\ \mu\text{m}$  orifice to produce a high velocity jet. This jet is injected through a vented chamber where it entrains air prior to combustion, similar to Premixed1. The fuel air mixture is then injected into a small combustion chamber of depth  $\delta_{light} = 3\ \text{mm}$ , where it is ignited by a piezoelectric spark device. This lighter does not use a flame stabilizer as described in Premixed1, and much of the combustion occurs outside of the chamber as illustrated in Figure 8. The geometry of the nozzle results in a different flame compared to Premixed1. These differences become apparent in the results. Details of the design characteristics are listed in Table 1. No design modifications were made to the nozzle or burner geometry in the test configuration.

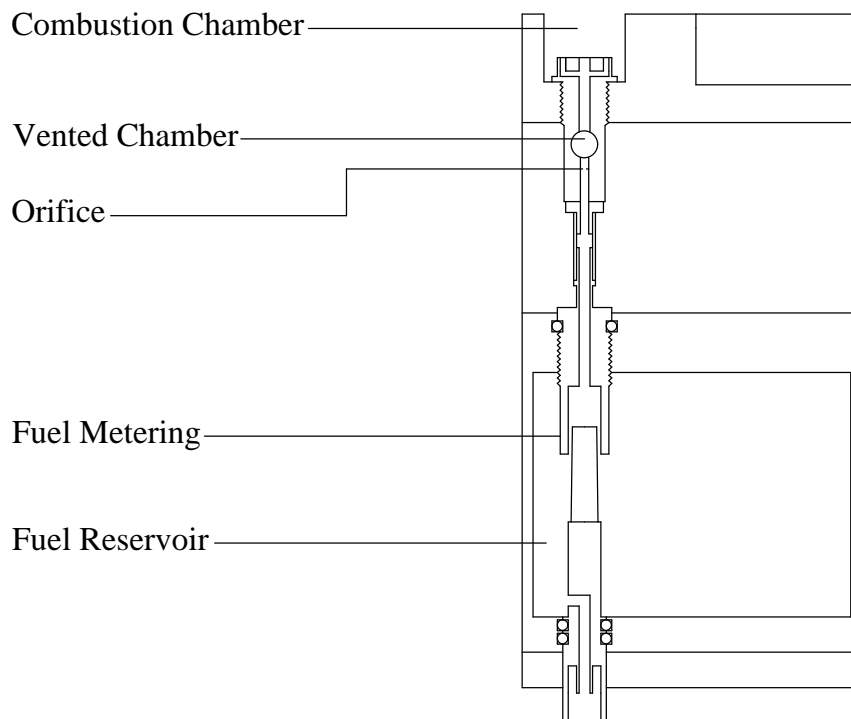


Figure 6: Scale drawing of a commercial Premixed2 Cigarette Lighter.

#### **2.1.1.4 Prototype Lighter**

This lighter was developed based on characteristics of the previous three nozzles that demonstrated improved unwanted ignition propensity or a need for improvement. This design utilizes the same nozzle used by Premixed1; however, the combustion chamber is different. The combustion chamber consists of three concentric, vented stainless steel tubes linked together using setscrews, and a wire mesh flame stabilizer as illustrated in Figure 7. Vented tubes (offset vents, 3.2 mm diameter on Tube 1 and Tube 2 and 4.8 mm diameter on Tube 3, spaced at 3.2 mm on center and at 60 degree intervals) were required to reduce velocities within the tube for flame stabilization. When the tubes were not vented, the flame propagated rapidly away from the point of ignition, rapidly expelling burning gasses out the end of the tube followed by flame extinction. By introducing vented tubes, the flame speed was reduced significantly resulting in a stable flame. This flame is completely contained within the combustion chamber leaving no visible combustion, as illustrated in Figure 8. The inner tube was designed to accommodate the outside diameter (8 mm) and length (83 mm) of a standard filtered cigarette. The inner tube acts as a heat sink that absorbs a portion of energy produced by the flame. In the previous cases, all of the energy released by the flame was convected away by the hot gasses in the plume. In this case, some of the energy is conducted away by the steel tube and the remaining energy is convected away by the hot gasses. The principle behind this design is that when the energy capacity of the hot gasses is reduced, the ignition propensity of those hot gasses will also be reduced. The energy conducted away by the inner tube is gradually released by natural convection and radiation to the outer two tubes. The

three-tube configuration was observed based on qualitative observations of surface temperature of the outer tube. In the two-tube configuration, the surface temperature of the outer tube increased to the threshold of pain much more rapidly than in the three-tube configuration. This performance characteristic led to fabrication of a simple model. This model predicts surface temperatures of the prototype based on inputs defined by the user. The user can modify inputs in order to predict the design with the best performance. The model is a one-dimensional heat transfer model with two zones for each tube. The lower zone is the region below the flame stabilizer and the upper zone is the region above the flame stabilizer. The two zones communicate through a simple conduction assumption. Energy is transferred between the tubes by convection and radiation using equations and methods described by Incropera.<sup>26</sup> Surface temperatures of each tube are calculated iteratively to simulate non-transient heat transfer. Inputs and equations used in the model will be explained in greater detail in the results. Some geometric design characteristics of the Prototype are listed in Table 1. A proposed cigarette lighter design utilizing the Prototype concept is illustrated in Appendix B.

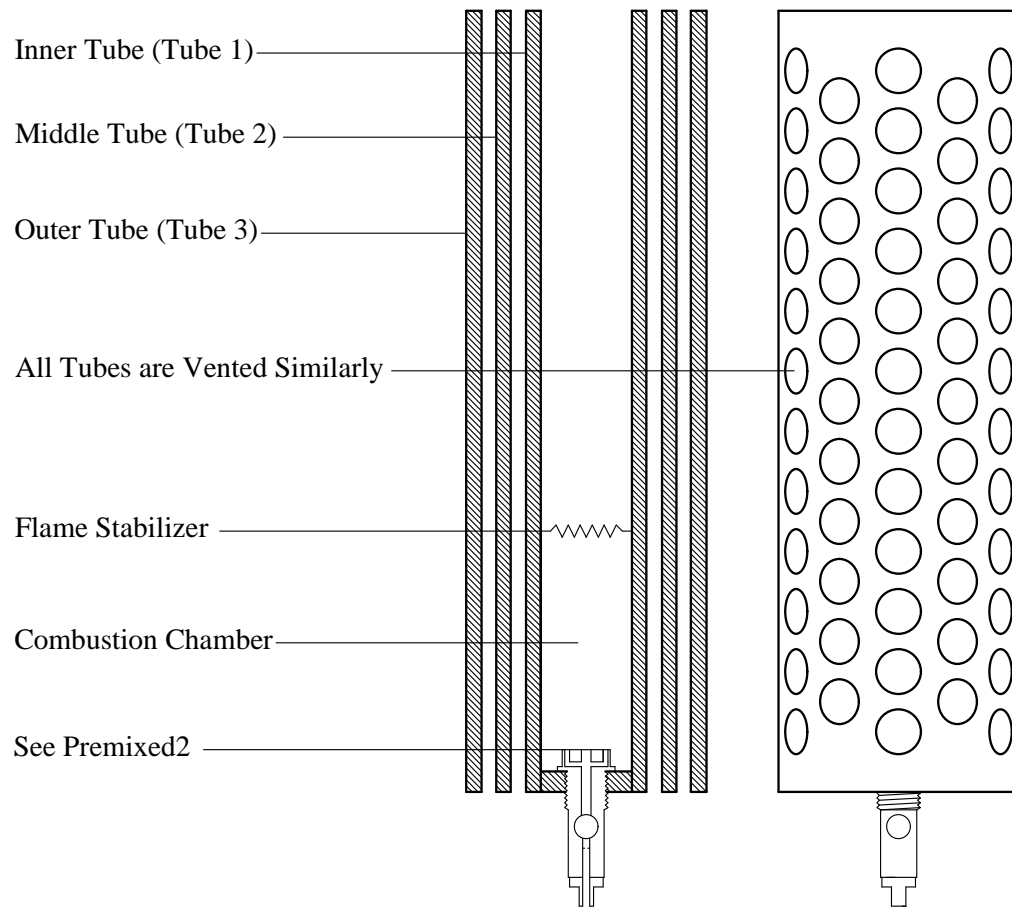


Figure 7: Scale drawing of the Prototype cigarette nozzle.

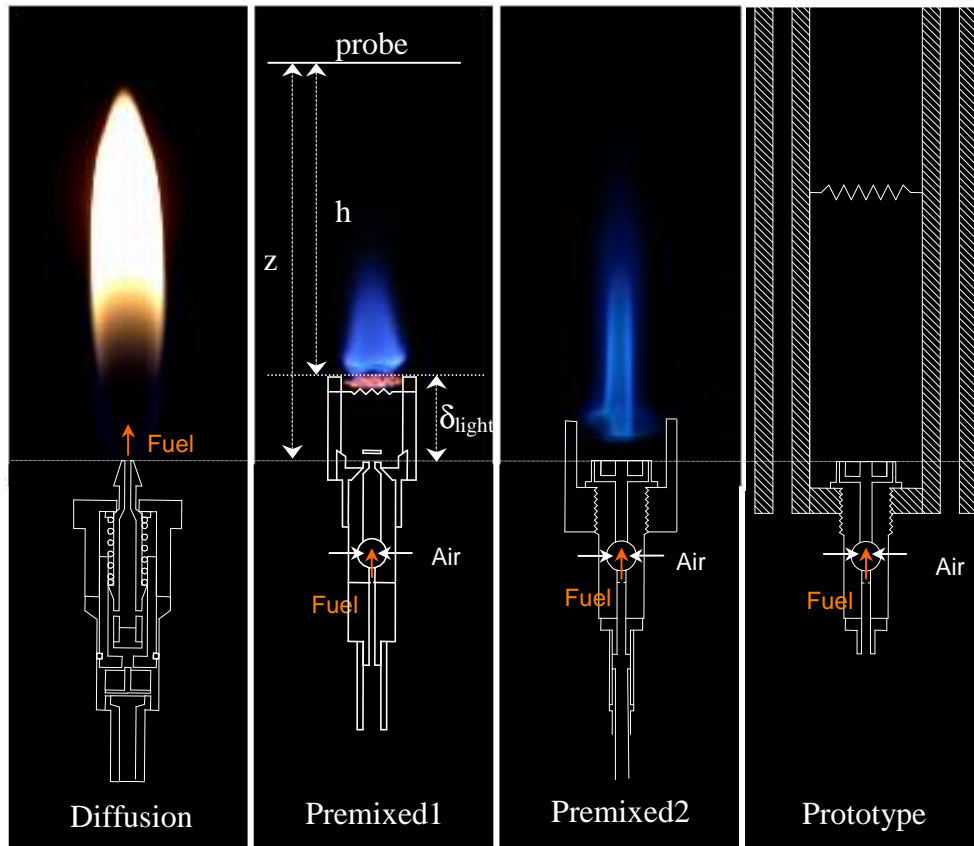


Figure 8: Nozzles with corresponding images of visible flames height above the exit plane,  $h$ , height above the source,  $z$ , and height of the combustion chamber,  $\delta_{light}$ , are illustrated graphically. No flame is visible in the Prototype.

Table 1: Key nozzle physical characteristics

Lighter Designation	Burner Type	Flame Stabilizer	Recession Depth, $\delta_{light}$ (mm)	Fuel Injection Diameter (mm)
Diffusion	Port	No	0	.5
Premixed1	Bunsen	Yes	6	.07
Premixed2	Bunsen	No	3	.07
Prototype	Bunsen	Yes	80	.07

### 2.1.2 Key Operation Parameters

The key parameters that remained constant during testing were the energy release rate of the flame, fuel type, and the vertical orientation of the lighter flame. The vertical orientation was necessary in order to accurately sample data at the centerline of the plume at all heights. Butane fuel was selected because it is the consensus fuel type for, adjustable, refillable, gas cigarette lighters. Liquid fuel lighters, such as Zippo® lighters, were not examined because the flame is considered to behave similarly to the standard butane diffusion lighter. The selected energy release rate of the flame was determined through qualitative analysis of ASTM F400-00 from flame height requirements for diffusion lighters, and the characteristic flow limitations of the actual cigarette lighters as they were purchased commercially. The ASTM standard dictates that the maximum flame height of adjustable diffusion lighters is 120 mm at the highest flow setting, and 75 mm for premixed lighters.<sup>4</sup> Preliminary qualitative testing, using the commercial designs, showed flow rates from Premixed1 and Premixed2 had mass flow rate upper limits of  $1.6 \times 10^{-6}$  kg/s and  $1.8 \times 10^{-6}$  kg/s, with corresponding flame heights of 20 mm and 15 mm respectively, while the diffusion lighter had no apparent limiting flow rate. All three of the lighters complied with ASTM F400-00, however the diffusion lighter could easily be modified to produce a non-compliant flame. Based on this information,  $1.5 \times 10^{-6}$  kg/s was an achievable and characteristic fuel mass flow rate for each of the selected lighter designs, corresponding to an energy release rate of 75 Watts using Equation (5) (Section 2.2.1). The flame heights associated with this energy release rate are 20

mm, 10 mm, and 15 mm for Diffusion, Premixed1 and Premixed2 respectively. This setting is well within the requirements prescribed by ASTM F400-00.

## **2.2 Experimental Apparatus**

The test facility as illustrated in Figure 9, was designed to produce a constant energy release rate while varying the cigarette lighter nozzle type. In order to achieve these characteristics, materials and processes were used that would allow for precise measurements in a small sampling region. To ensure constant energy release rate, the mass flow rate of the fuel must be constant and reproducible. The fuel was gaseous butane stored as a saturated liquid in a small pressure vessel. A pressure regulator was used to ensure that the fuel was supplied at a constant pressure of 69 kPa. A precision metering valve with a Vernier scale ( $\pm 0.01$  turns with 2 turns from open to closed) was used to control the flow rate. The pressure regulator and metering valve were designed to mimic the pressure drop achieved internally by the portable designs available in commercial cigarette lighters. In preliminary testing, the fuel nozzles had a tendency to increase in temperature with time. As the temperature of the nozzle increased, thermal expansion caused a variation in the diameter of the orifice in Premixed1 and Premixed2. The diameter of the orifice has a significant effect on the mass flow rate of the fuel, therefore the temperature of the nozzle must be maintained near room temperature to reduce the variation of the mass flow rate with time. A water-cooled clamp was introduced to maintain the nozzle at a constant temperature, and for mechanical stability, as illustrated in Figure 10.

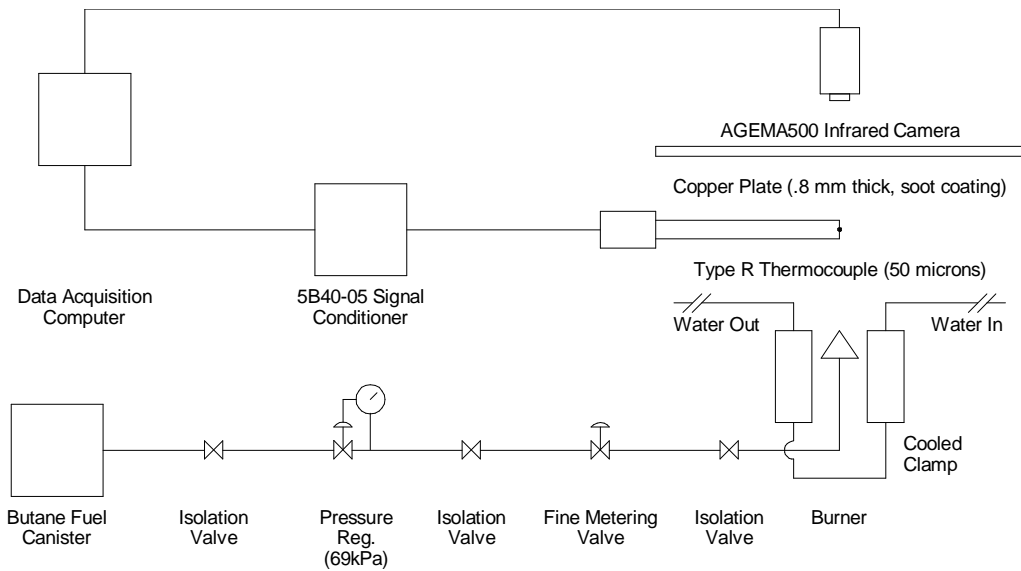


Figure 9: Experimental setup: diagnostic systems (top) and fuel system (bottom).

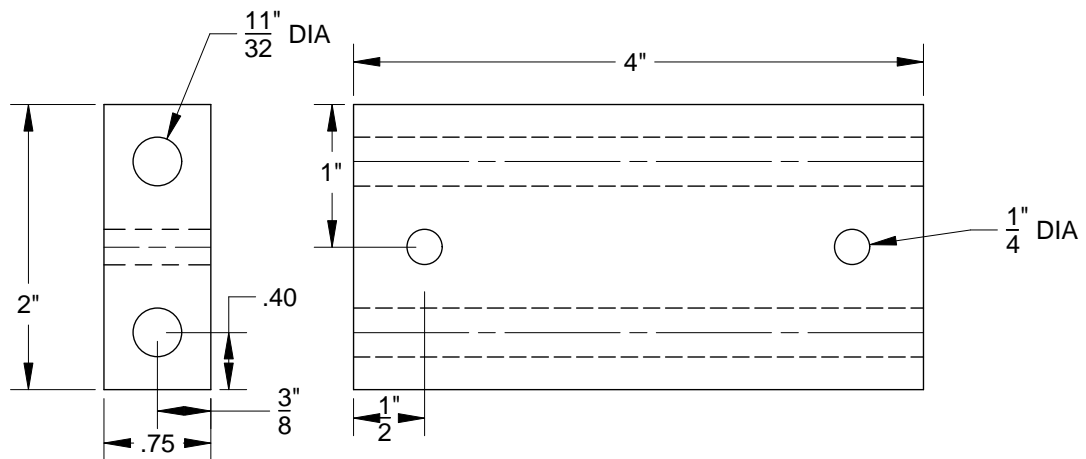


Figure 10: Illustration of one side of the water-cooled clamp. Water is circulated length-wise through both sides of the clamp to achieve cooling.

### 2.2.1 Flow Calibration

With the aforementioned flow metering features in place, flow calibrations were performed for each lighter nozzle tested. Prior to each test, the mass of the fuel vessel was measured with a high-accuracy mass scale ( $\pm 10^{-4}$  grams). The nozzle was then operated for a long period of time measured with a stopwatch from the opening of the fuel flow to the closure of the fuel flow. During the test, the flame was observed to ensure that there were no significant variations in size, shape or color, which would indicate a change in the energy release rate of the flame. After each test, the mass of the fuel vessel was measured again and the mass flow rate was determined from the mass loss and the time of operation by a simple calculation:

$$\dot{Q} = \Delta h_c \dot{m} = \Delta h_c \frac{\Delta m}{\Delta t}, \quad (5)$$

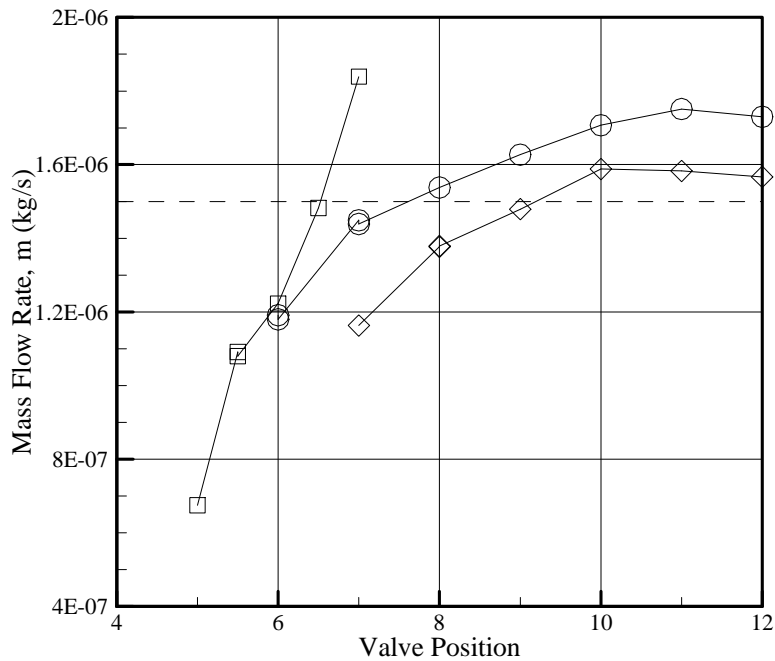


Figure 11: Flow calibration data where the dashed line indicates the desired mass flow rate associated with 75 W, the Prototype is the same as Premixed2.  
 □ - Diffusion, ○ - Premixed1, ◇ - Premixed2.

Where  $\Delta h_c = 45,690$  kJ/kg for butane. The test was performed at different settings of the fine metering valve until the setting that produced the mass flow rate corresponding to 75 Watts was obtained. Calibration results are illustrated in Figure 11. The valve settings were different for the various nozzle types because of different internal restrictions and the associated pressure drops for each nozzle.

### **2.2.2 Stability and Alignment**

Once the flow system was established, a system was constructed to mount diagnostics above the source such that they would measure centerline characteristics of the plume at any height. A vertically mounted Velmex A1509K1M-S1.5 Vernier scale traverse mounting system was selected, with an accuracy of  $\pm 10^{-4}$  m, such that it could be easily connected to any diagnostic device. The traverse was aligned with a plum line, and careful attention was given to ensure that the fuel nozzle was also vertically aligned. Alignment was evaluated by determining the position of the centerline of the plume at multiple heights by imaging a horizontal flat copper plate with an IR camera as described in Section 2.3.2. When the location of the centerline was the same at all heights, the nozzle was perfectly aligned. In order to achieve stability in alignment, a double enclosure was built around the test facility to limit ambient instabilities.

### **2.3 Diagnostics**

There were three main diagnostics used to evaluate the ignition propensities of the nozzles. Diagnostic tools were designed that would measure centerline plume

temperature, heat flux to a horizontal flat plate, and ignition propensity of a selected material. These diagnostics produce highly accurate results in a small-scale flame, such that the data taken could be compared to existing data from larger scale fire tests.

### 2.3.1 Temperature and Transition to Turbulence

The temperature diagnostics consisted of a type-R micro-thermocouple connected to a signal conditioner and read by a data acquisition computer. A small micro-thermocouple (50  $\mu\text{m}$  diameter) was selected because it produced the accuracy desired for temperature measurements. It was less likely to disturb the plume than a larger thermocouple, and the probe was designed to be unobtrusive to the flow, as illustrated in Figure 12.<sup>27</sup> It had a low time response of 27 ms for accurate measurement of the turbulent fluctuations that occur below 37 Hz. A sampling rate of 100 Hz was selected to fully characterize the response of the thermocouple. Power spectra analysis showed that very little power occurred at frequencies higher than 37 Hz, illustrating that the thermocouple accurately represents the instantaneous gas temperature along the centerline of the plume. Another benefit of a smaller thermocouple is the reduced affect of radiative losses however; the data was corrected for radiation by calculating the energy balance to the thermocouple bead using the following equation:<sup>15</sup>

$$T = \frac{\sigma \epsilon}{h_c} (T_{tc}^4 - T_{\infty}^4) + T_{tc}, \quad (6)$$

Where  $T$  is the corrected thermocouple temperature,  $\sigma$  is the Stefan Boltzman constant,  $\varepsilon = 0.1$  for platinum,  $T_{tc}$  is the recorded thermocouple temperature, and  $h_c$  is determined by heat transfer correlations from Incropera et al.:<sup>26</sup>

$$Nu_d = \frac{h_c d}{k_{air}} = 2 + (0.4 Re^{1/2} + 0.06 Re^{2/3}) Pr^{2/5}, \quad (7)$$

Where  $d$  is the diameter of the thermocouple bead,  $Pr = .68$  for air and the Reynolds number is:

$$Re = \frac{ud}{\nu_{air}}, \quad (8)$$

Where  $\nu_{air}$  is the kinematic viscosity of air, and  $u$  is the velocity of the plume as correlated by Morton et al.:<sup>5</sup>

$$u = 3.9 \left( \frac{g \dot{Q}}{T_{\infty} c_p z} \right)^{1/3}, \quad (9)$$

Where  $c_p$  is the specific heat of air, and  $z$  is the height above the source. The thermocouple was connected to a National Instruments (NI) 5B40-05 signal conditioner, which magnified the signal from the device and simultaneously filtered the background electrical noise measured, improving the signal-to-noise ratio. The signal conditioner was connected to the data acquisition computer via a NI PCI-MIO-16XE-50 board, which converted the signal to digital data using NI Lab View software program (Appendix C), specialized for high frequency thermocouple measurements. Centerline temperatures were calculated as the time average (mean) value of the sampling period of 100 s to 300 s, increasing with height. Average temperature measurement is based on a steady state combustion condition.

Temperature standard deviation was also calculated and used as an indicator for

transition to turbulence. In the case of the Prototype nozzle, the steady state condition occurred after a long period of operation when all three tubes reached a steady state temperature. This dictates that the prototype nozzle be thermally isolated from the tubes to ensure that its temperature remains constant, because the flow calibrations rely on maintaining a room temperature nozzle. Regulation of the nozzle temperature was achieved using a water-circulating micro-cooling device that mounted the nozzle to Tube 1, as illustrated in Figure 13.

### 2.3.2 Heat Flux to a Horizontal Flat Plate

The heat flux diagnostics consisted of an Infra Red (IR) Camera (Agema 550) connected to a data acquisition computer using a frame grabber program. The camera imaged a thin flat copper plate (30.5 cm × 28 cm × 0.08 cm), uniformly coated with a thin film of soot to ensure a constant and known surface emissivity ( $\epsilon = 0.95$ ), held horizontally in the plume. Copper was selected for its high thermal conductivity to ensure a nearly uniform temperature over the thickness of the plate. The plate was imaged at 10 Hz for 30 seconds. The digital thermal images provide high-resolution

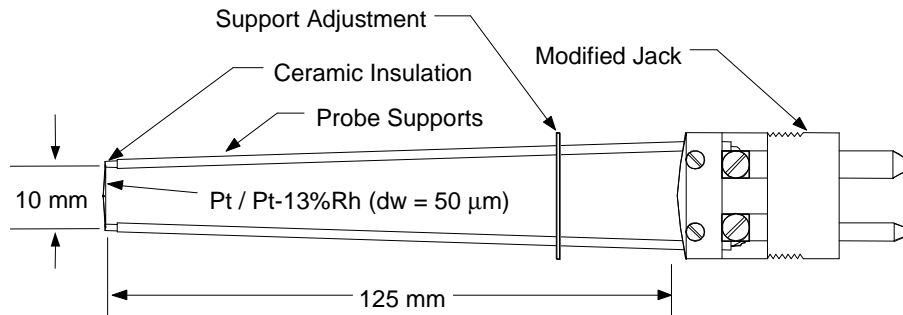


Figure 12: Thermocouple probe design.<sup>27</sup>

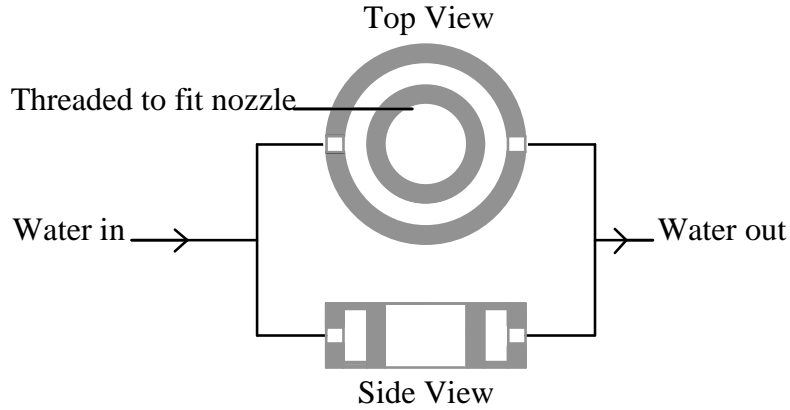


Figure 13: Water-cooling device for the prototype nozzle.

temperature data from 0.6 mm/pixel to 0.8 mm/pixel, depending on the field of view with an image size of  $240 \times 320$  pixels. The images were then time and spatially averaged (mean), assuming that the flow is axis-symmetric. From the average data, the location of the peak temperature of the plate was determined. Temperatures were recorded outwardly from that point in the positive and negative x and y directions. These four temperatures were again averaged and used as the temperature data for each sampling height. The temperature data were reduced to a best-fit function similar in form to the equation used by Veldman et al.:<sup>10</sup>

$$T(R) = \frac{C_1 R^4 + C_2 R^3 + C_3 R^2 + C_4 R + C_5}{C_6 R^4 + C_7 R + 1}, \quad (10)$$

where  $R = r^2$  as illustrated in Figure 15. The processed temperatures were then analyzed with a numerical Matlab code illustrated in Appendix D, that solved for the heat flux to the plate at a radial position, using an energy balance method described by Zukoski:<sup>25</sup>

$$\dot{q}_{in} = \dot{q}_{cond,netout} + \dot{q}_{conv,out} + \dot{q}_{rad,out}, \quad (11)$$

A graphical representation of this energy balance model is illustrated in Figure 14.

Application of Newton's law of cooling, Fourier's law, and the Stefan-Boltzmann law yields:

$$\dot{q}_{in}'' = -\frac{kt}{r} \left( \frac{\partial T_p}{\partial r} + r \frac{\partial^2 T_p}{\partial r^2} \right) + h(T_p - T_{amb}) + 2\varepsilon\sigma(T_p^4 - T_{amb}^4), \quad (12)$$

Equation (2) is transformed in order to avoid the singularity at  $r = 0$ . This singularity prevents estimation of the stagnation point heat flux. The transformation variable  $R$

$= r^2$  provides:

$$q_{in}'' = -4kt \left( \frac{\partial T_p}{\partial R} + R \frac{\partial^2 T_p}{\partial R^2} \right) + h(T_p - T_{amb}) + 2\varepsilon\sigma(T_p^4 - T_{amb}^4), \quad (13)$$

where the convective heat transfer coefficient,  $h$ , was determined from Incropera:

$$\overline{Nu}_L = 0.15Ra_L^{1/3}, \quad (14)$$

where  $L \equiv A_s/P$  and  $Ra_L$  is based on an average (mean) plate temperature.<sup>26</sup> The image averaging and best fit were necessary to reduce noise in the data because the derivative of Equation (9) could be evaluated exactly. The numerical method developed for evaluating the empirical heat transfer equations, Equation (11), was very sensitive to low levels of noise in the data, such that reliable numerical differentiation was impossible. The combination of each of the methods used in this formulation allowed for very precise calculations of the heat flux with radial position, even at the stagnation point.

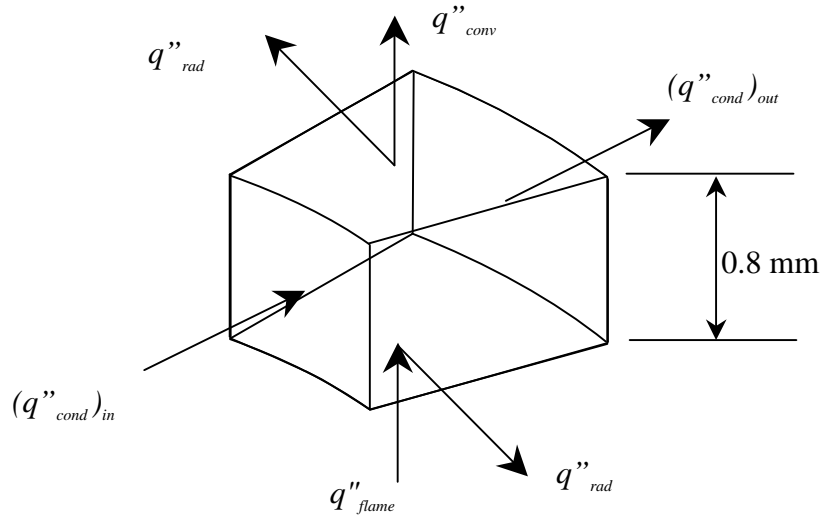


Figure 14: Illustration of the radial energy balance of a section of the copper plate.

### 2.3.3 Ignition of Filter Paper

While the heat flux measurements provided a quantitative basis for assessing the unwanted ignition risk from the lighters used in this study, the ignition tests provide context for these measurements. Ignition testing alone however, is not a good indicator for ignition propensity of actual combustibles. There can be a wide range of ignition performance from material to material in actual use, and it would be incorrect to assume that the results of ignition data taken with only one combustible material would be representative of that of all other materials.

Filter paper was selected because of its availability, low expense, thermally thin characteristics, repeatability, and ease of use. The ignition experiments were designed such that the filter paper was mounted as horizontal flat plate geometry. This ensured that the heat flux to the surface was the same as in the case of the heat

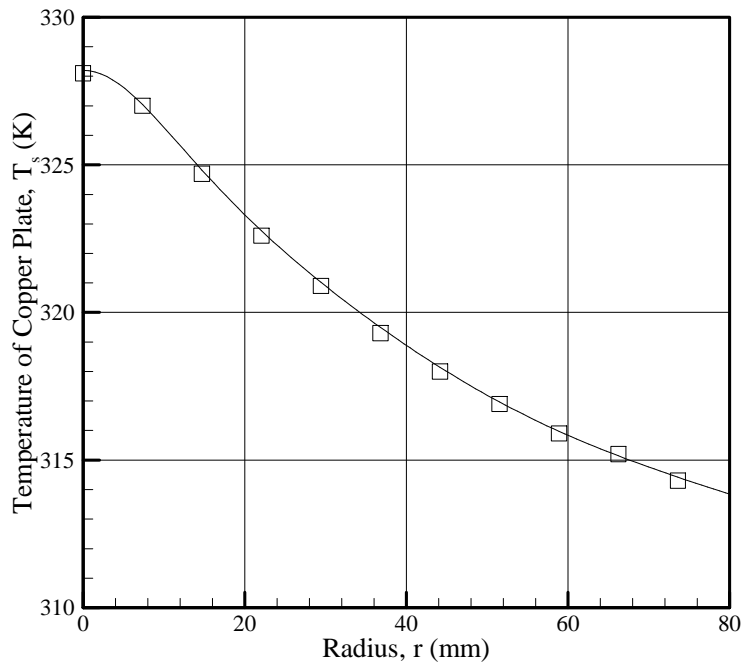
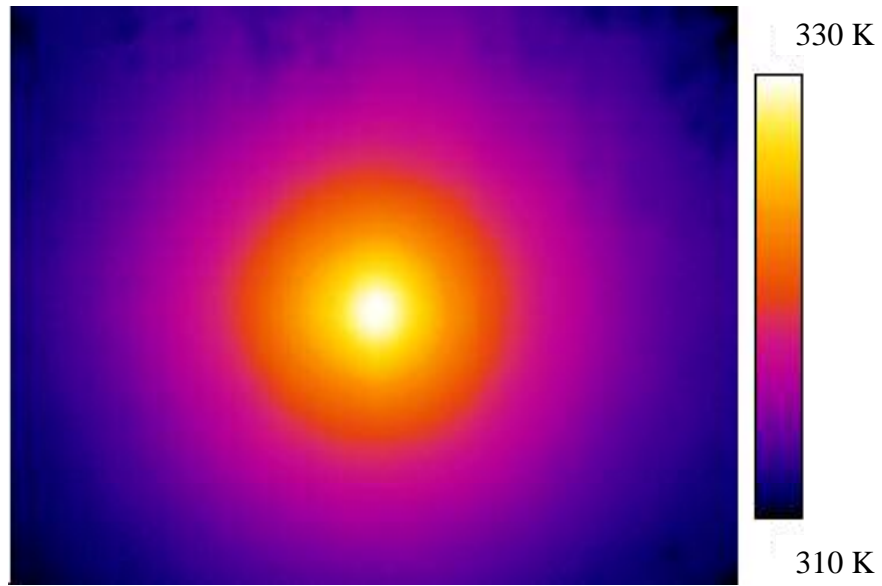


Figure 15: Sample IR image (top) with associated best-fit temperature profile (bottom).

flux diagnostics. Ignition was determined visually as either the appearance of flame or smoldering, as indicated by glowing of the filter paper. A stopwatch, starting at the onset of exposure of the filter paper to the hot gasses and stopping at visual ignition, measured the time to ignition. This method was repeated three to five times at each height, and averaged. A critical height was determined from this data as the maximum height of ignition and given the designation  $(h_{ig})_{crit}$  tabulated for each lighter. This ignition time was then compared to the incident heat flux data to evaluate a critical ignition heat flux for the filter paper.

## **2.4 Summary**

The experimental approach resulted in very accurate and highly resolved data for each of the desired thermal characteristics. Such high resolution was needed to fully characterize the scales associated with cigarette lighter flames. This also allowed for a detailed comparison of unwanted ignition propensity from each of the nozzles tested. Data from each of the nozzles were collected and important performance characteristics were derived from its analysis.

## Chapter 3: Results

### 3.1 Characterizing Existing Cigarette Lighters

Three cigarette lighter nozzles were tested in order to characterize the ignition propensity of existing cigarette lighters. Each lighter is designated as Diffusion, Premixed1, Premixed2 and Prototype and is illustrated in Figures 4-7. Figure 8 illustrates the visible flames produced by these lighters, as well as an illustration of the definitions of  $h$  and  $z$ . Temperature measurements, heat flux measurements and filter paper ignition measurements were performed to characterize the ignition propensity of those devices. A comparison of the performance of each of these lighters will illustrate design characteristics of each nozzle that demonstrate improved unwanted ignition propensity or a need for improvement.

#### 3.1.1 Flame Height

The flame height,  $h_f$ , is an important flame characteristic related to the lighter ignition propensity. Ignition characteristics are expected to be quite different in the flame region than in the plume region. Flame heights with respect to the lighter exit plane,  $h = 0$ , corresponding to the three lighters with visible flames were determined optically from Figure 8. The corresponding flame heights for each nozzle are:  $h_f = 20$  mm for Diffusion,  $h_f = 9$  mm for Premixed1, and  $h_f = 15$  mm for Premixed2. Each nozzle produces a different flame height based on their geometry and the type of combustion. The Diffusion nozzle produces the longest flame height because the fuel air mixing is limited by diffusion, making the reaction zone longer. Premixed1 produces a dramatically shorter flame height based on the geometry of the burner, and

corresponding fuel-air mixing. Part of the flame exists within the combustion chamber as illustrated in Figure 8, and only the unburned fuel reacts outside of the nozzle, greatly reducing the visible flame height measured from the lighter exit plane. Premixed2 produces a much longer flame height than Premixed1 because of its geometry. The Premixed2 nozzle creates a partially premixed flame with a fuel rich center. This partially premixed central core reacts more slowly than the well-mixed Premixed1 lighter, resulting in a longer reaction zone. For scaling purposes, a flame height with respect to the source will be the appropriate length scale such that  $z_f = h_f + \delta_{light}$ . The flame heights based on the source datum are  $z_f = 20$  mm,  $z_f = 15$  mm, and  $z_f = 18$  mm for Diffusion, Premixed1 and Premixed2 respectively as noted in Figure 8, where values for  $\delta_{light}$  are listed in Table 1.

### 3.1.2 Temperature

Average centerline temperatures were measured using a micro-thermocouple and adjusted for radiation losses. Adjusted temperature data is illustrated in Figure 16; maximum temperature adjustments were approximately 70 K. Clearly, each nozzle has drastically different centerline temperature behavior in the near field. The Diffusion flame produces a temperature of 1032 K at a height of  $h = 1.0$  mm, gradually increasing to a peak temperature of 1930 K at  $h = 19.0$  mm just below the flame height  $h_f = 20$  mm. This temperature is near the adiabatic flame temperature for butane. It is slightly lower due to radiative heat losses from the flame. The Premixed1 flame produces a nearly constant temperature reaction zone within the flame where the peak temperature is 1763 K at  $h = 1.0$  mm and 1700 K at  $h = h_f =$

9.0 mm. The Premixed2 flame produces a strange centerline temperature behavior. Near the exit plane, the temperature behavior is similar to that of the flame zone described for Premixed1 such that there is a nearly constant temperature initially ranging from 1687 K to 1724 K for  $1.0 \text{ mm} < h < 3.5 \text{ mm}$ . There is a rapid decrease in temperature between  $h = 3.5 \text{ mm}$  and  $h = 4.5 \text{ mm}$  before the temperature begins to behave similarly to that of the Diffusion nozzle with a maximum temperature of 2022 K at  $h = 13.5 \text{ mm}$  just below the flame height. This behavior suggests a premixed reaction in the near field and mixing controlled reaction further downstream of the source. This behavior is characteristic of partially premixed flames. The temperature profile of each nozzle illustrates rapid temperature decay at locations above the flame height.

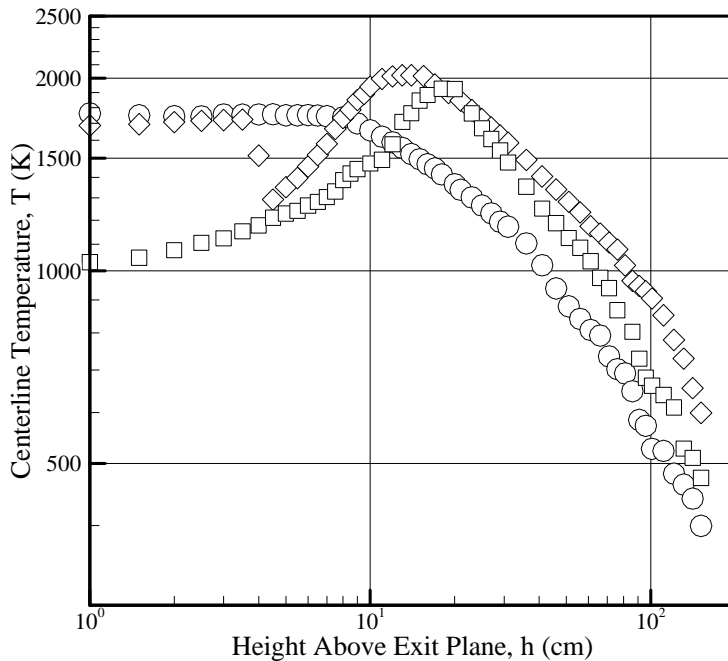


Figure 16: Centerline temperature profiles for the three existing cigarette lighter nozzle designs.  $\square$  - Diffusion  $\circ$  -Premixed1  $\diamond$  -Premixed2

Based on the data illustrated in Figure 16, a scaling analysis can be performed for a comparison to existing data. Morton et al. has performed scaling analysis on the flow equations for fire plumes, and McCaffrey has tabulated data from several fire tests illustrating  $z^* \sim \theta^{-5/3}$  relationship between dimensionless temperature and dimensionless height where the dimensionless temperature is defined as:

$$\theta = \frac{T - T_\infty}{T_\infty} \quad (15)$$

and the dimensionless height is defined as:

$$z^* = \frac{z - z_0}{D^*} \quad (16)$$

where  $z$  is illustrated in Figure 8, the virtual origin of the source  $z_0$  is calculated using a method prescribed by Quintiere, and  $D^*$  is a characteristic length scale defined as:

$$D^* = \left( \frac{\dot{Q}}{\rho_0 c_p T_\infty g^{1/2}} \right)^{2/5} = 21.5 \text{ mm} \quad (17)$$

Where  $\rho_0$  is the density of air, and  $c_p$  is the specific heat of air.<sup>5,6,30</sup> The results of applying this scaling method to the data is illustrated in Figure 17.

The scaling of the data shows that for a sufficiently large  $z^*$  the temperature decays with the (-5/3) power law despite having significantly lower energy release rates (75 W) when compared to the experiments of McCaffrey (14.4 kW to 57.5 kW) and the correlation presented by Heskestad.<sup>6,30</sup> This suggests that far from the source, the flow becomes sufficiently turbulent to decay at the same rate as the fully turbulent pool fires tested by McCaffrey and Heskestad. Based on Figure 17, the dimensionless height where fully turbulent flow is observed is  $z^* \sim 3$  for Diffusion

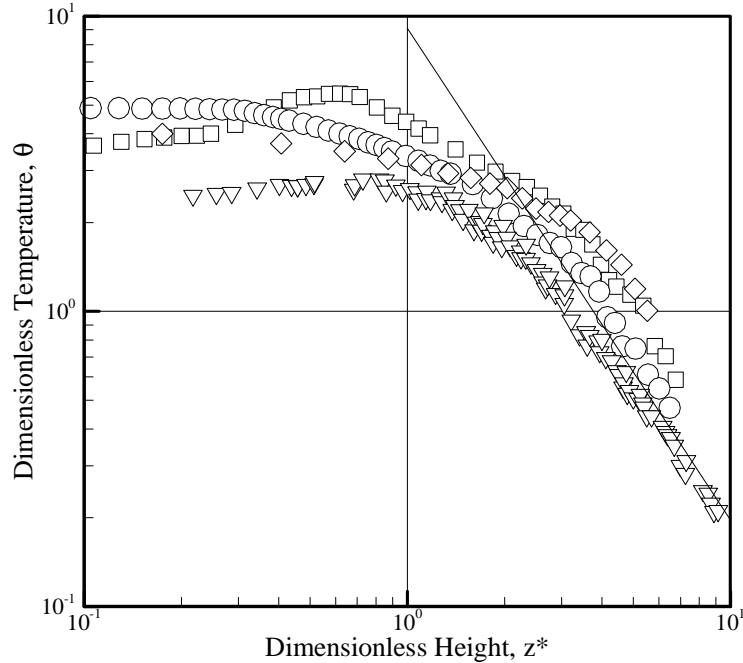


Figure 17: Scaling analysis of centerline temperature data compared to data from McCaffrey and a correlation presented by Heskestad,<sup>6,30</sup> indicating fully established turbulent flow behavior at  $z^* \sim 3-5$  for the conventional lighters.  
 □ - Diffusion   ○ - Premixed1   ◇ - Premixed2   ▽ - McCaffrey   — Heskestad

and Premixed1, and  $z^* \sim 5$  for Premixed2. This dimensionless height range,  $z^* \sim 3$  to 5 corresponds to  $Ra_q \sim 10^9$  using Equation (2). This value is consistent with the critical value presented by Bejan that the turbulent transition must occur at  $Ra_q < 10^{10}$ .<sup>23</sup> McCaffrey's data illustrates multiple regions indicated by different temperature decays. There is a constant temperature region which he calls the flame zone, and a transition region with a (-1) power law decay caused by the intermittent flame region.<sup>6</sup> The flames observed in this study do not all have constant temperature reaction zones because of the laminar flow condition. These flames do not have an intermittent flame zone as would be expected in turbulent pool fires, but there is an analogous temperature decay transition, which is thought to be due to a transition to

turbulent flow. More credible approximations for turbulent transition can be determined from fluctuating temperature measurements discussed below.

Although the  $(-5/3)$  power law decay is observed in the temperature rise data for each lighter, the temperature decay curves are not coincident as illustrated in Figure 17. These offsets are due to the higher flame temperatures achieved in laminar and weakly turbulent flames, which have significantly lower entrainment rates than fully turbulent flames. This effect is illustrated by variation of  $\alpha$  in Equation (1). The behavior prior to the  $(-5/3)$  decay is difficult to correlate because the contributing factors of mass flux, buoyancy flux, and momentum flux cause different flow behaviors as described by Morton. Morton calls this case the *forced plume*, and he describes the behavior generally as a flow that initially behaves like a jet, transitioning to plume behavior in the far field.<sup>8</sup> Reaction in the near field also changes the scaling, making correlation difficult. However, for the reacting plume, flames with lower entrainment will have higher temperatures, which is consistent with the observed trends.

The standard deviation,  $T'$  of each sample temperature measurement was also recorded. This data can be correlated as an indicator to transition to turbulence where the temperature fluctuation rapidly begins to increase. Figure 18 illustrates dimensionless temperature fluctuation, defined as

$$\theta' = \frac{T'}{T - T_\infty}, \quad (18)$$

Where  $T$  is the plume centerline temperature, versus dimensionless height,  $z^*$ . Figure 18 illustrates an increase in temperature fluctuation at  $z^* \sim 2$  to 3, which is slightly less than the prediction from the scaling analysis illustrated in Figure 17. This value

is expected to be less than that found from Figure 17 because fully established turbulent flow will occur slightly downstream from the onset of transition to turbulence. This corresponds to a turbulent transition height of  $z_t \sim 4.3$  cm to 6.5 cm with respect the source.

Analysis of mean temperature data may be used to make a comparison of ignition performance of the three nozzles tested. At this point, only temperature information is being considered, therefore the nozzle that produces the lowest gas temperatures will have better unwanted ignition propensity performance. The Premixed1 nozzle produced the lowest maximum temperature of the three nozzles. This nozzle produces a lower gas temperature because the geometry of the combustion chamber and the flame stabilizer act as a heat sink for the flame. Since the combustion chamber and the flame stabilizer absorb some of the energy release rate of the flame, less energy is convected away by the hot gasses, resulting in a lower gas temperature. This concept was explored in development of the Prototype nozzle. The caveat of this feature is that the surface temperature of the nozzle will increase due to heating from the flame. The surface temperature of Premixed1 was measured with thermocouples to reveal the surface temperature performance of the nozzle without the water-cooling clamp illustrated in Figure 10. The results of the Premixed1 surface temperature test are illustrated in Figure 19 for a fuel cutoff time of 110 s, and the peak surface temperature of the nozzle was 453 K at 110 s. This surface temperature seems unreasonably high, although typical shutoff times for lighters in actual use are much lower than 110 s, which would result in a correspondingly lower

surface temperature. This surface temperature data is an indicator of an acceptable surface temperature performance level for existing cigarette lighters.

### 3.1.3 Heat Flux

Heat Fluxes to a horizontal flat copper plate were calculated from IR imaging of the back side of the copper plate. A Matlab program, provided in Appendix D, was developed to solve Equation (13) for all  $R$ . The results were then transformed back to radial coordinates using the definition  $R = r^2$ . Using this methodology, the maximum heat fluxes were determined to be  $(\dot{q}_0'')_{\max} = 63 \text{ kW/m}^2$  for the Diffusion nozzle,  $(\dot{q}_0'')_{\max} = 169 \text{ kW/m}^2$  for Premixed1 and  $(\dot{q}_0'')_{\max} = 326 \text{ kW/m}^2$  for Premixed2. All peak heat fluxes occurred at the stagnation point of the impinging flow. The heat flux profiles corresponding to the maximum heat flux are illustrated in Figure 20. These profiles illustrate that the incident heat flux to the copper plate was highly

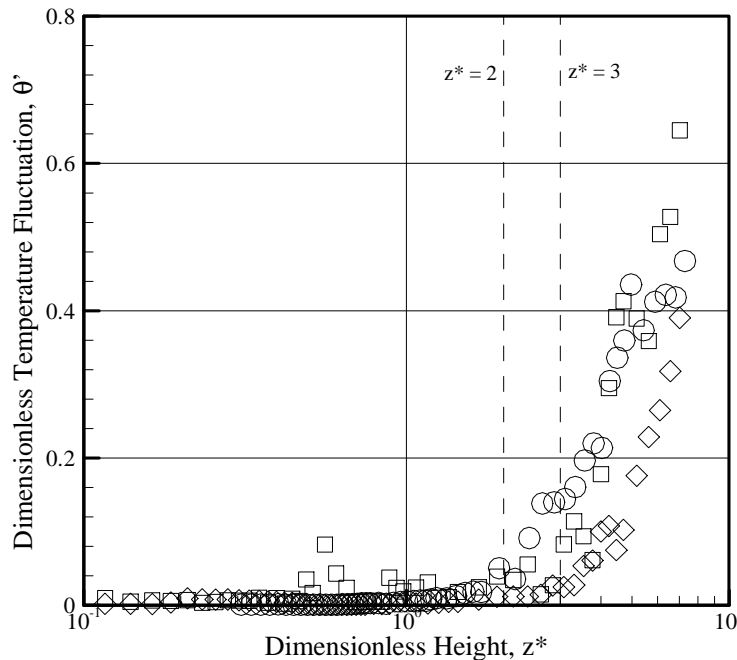


Figure 18: Scaling analysis of temperature fluctuations, indicating turbulent transition in the range  $z^* \sim 2-3$ .  $\square$  - Diffusion  $\circ$  - Premixed1  $\diamond$  - Premixed2

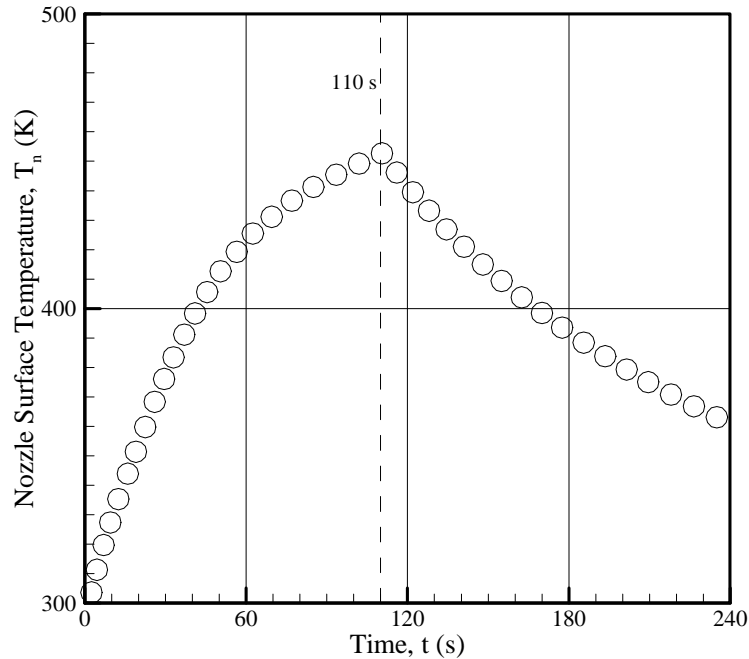


Figure 19: Premixed1 surface temperature performance for 110 s of operation without the water-cooling clamp.

concentrated near the stagnation point, especially for Premixed1 and Premixed2. The Diffusion flame produces a lower peak heat flux, but affects a larger area than the other two. At each sampling height, the peak incident heat flux occurred at the stagnation point. Figure 21 illustrates the stagnation point heat flux versus height. In this figure, the dashed line indicates a critical heat flux of  $50 \text{ kW/m}^2$  discovered from ignition of filter paper as described below. Integral analysis of the heat flux profiles illustrated that the total energy transferred to the surface varied with height, and ignition scaling based on the area of exposed heating was inconclusive. The maximum heat flux is most indicative of a worst-case scenario for ignition. All nozzles illustrate a generally decreasing incident heat flux with the ceiling height.

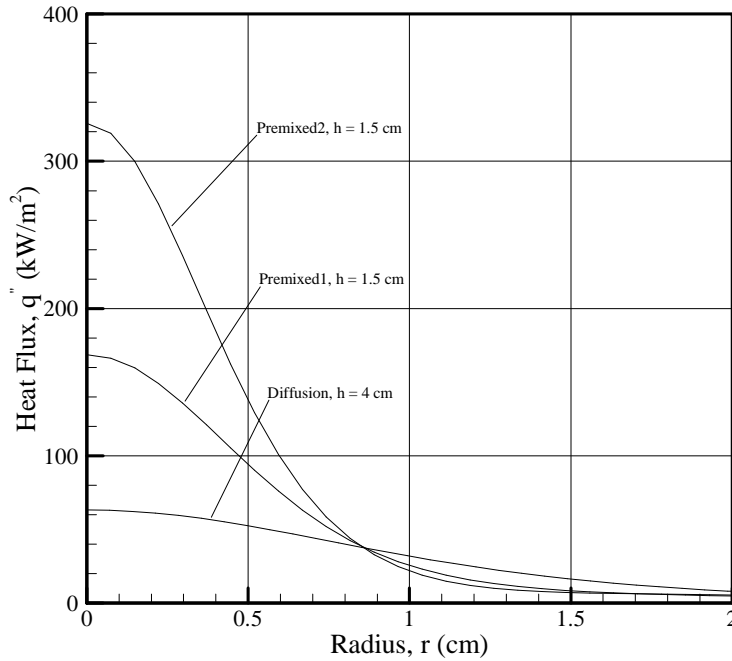


Figure 20: Heat flux profiles corresponding to the maximum observed incident heat flux.

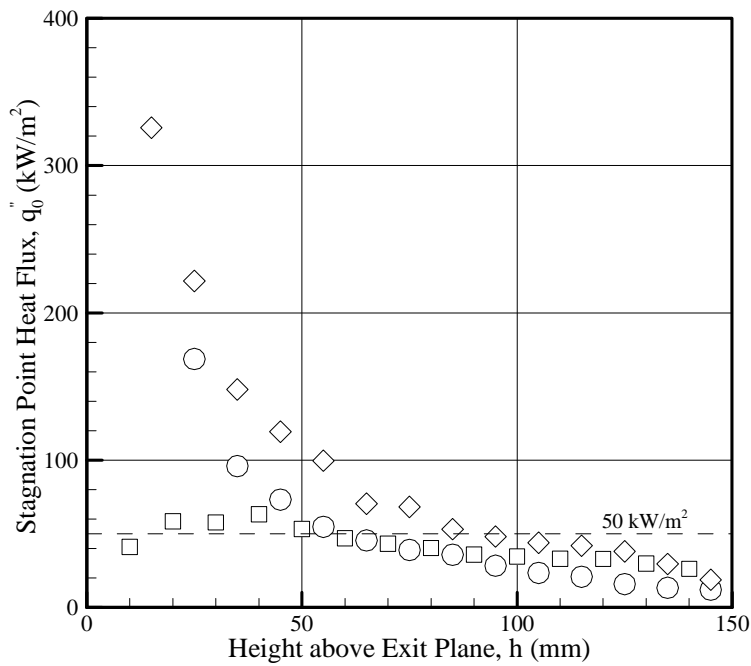


Figure 21: Stagnation point heat fluxes as a function of height, with a dashed line indicating  $50 \text{ kW/m}^2$  as a critical heat flux determined from ignition of filter paper.  
 □ - Diffusion   ○ - Premixed1   ◇ - Premixed2

Scaling analysis of the heat flux data can be performed to illustrate agreement of the data with theoretical predictions. Kokkala has presented a method for scaling heat flux data using  $\xi Ra_q^{1/6}$ , where  $\xi$  is defined by Equation (3) and  $Ra_q$  is defined by Equation (2), and a dimensionless height defined by  $z/z_f$ .<sup>28</sup> However, the data from the three nozzles does not correlate well using this scaling method. A new scaling term,  $\xi Ra_q^{-3/8}$  was determined from Williamson and Marshall, assuming laminar flow and laminar stagnation point theory following Faeth and You.<sup>29,11</sup> The method for determining this scaling parameter follows:

$$\dot{q}_s'' \propto \text{Pr}^{-3/5} v^{1/2} c_p \rho (T - T_w) \left[ \left( \frac{dv}{dr} \right)_{r=0} \right]^{1/2}, \quad (19)$$

where Pr is the Prandtl number,  $T_w$  is the wall temperature, and  $v$  is the flow velocity:

$$\frac{dv}{dr} \propto \frac{v_c}{r_{1/e}}, \quad (20)$$

where  $v_c$  is the characteristic velocity of the flow at radius  $r_{1/e}$  or the plume width.

Substitution yields:

$$\dot{q}_s'' \propto (T - T_w) \left( \frac{v_c}{r_{1/e}} \right)^{1/2}, \quad (21)$$

recognizing that:

$$Q \propto \rho c_p r_{1/e}^2 v_c (T - T_w), \quad (22)$$

substitution yields:

$$\dot{q}_s'' \propto Q v_c^{-1/2} r_{1/e}^{-5/2}, \quad (23)$$

where laminar plume scaling from Bejan illustrates:

$$v_c \propto \frac{Ra_q^{1/2}}{z}, \quad (24)$$

and:

$$r_{1/e} \propto z Ra_q^{-1/4}, \quad (25)$$

such that substitution and arrangement yields:

$$\frac{\dot{q}_s'' z^2}{Q} Ra_q^{-3/8} = \xi Ra_q^{-3/8} \propto 1, \quad (26)$$

as the appropriate scaling parameter for laminar stagnation point heat flux to a horizontal flat ceiling.<sup>23</sup> The data correlates to an order of magnitude as illustrated in Figure 22 as long as  $z/z_f$  is greater than unity. This scaling illustrates laminar flow at all heights for impingement to a horizontal flat ceiling, despite the indication of turbulent transition in the range of  $4.3 \text{ cm} < z < 6.5 \text{ cm}$  predicted from temperature fluctuation measurements without a ceiling. The possibility of laminar condition is not entirely unrealistic because the calculated  $Ra_q < 10^{10}$  which is the critical transition limit prescribed by Bejan.<sup>23</sup> In fact, introduction of the flat plate was observed by shadow graphing to increase the stability of the flow, allowing the turbulent transition height to increase as illustrated in Figure 23.

This heat flux information can be used to compare unwanted ignition propensity from each lighter. Flammable materials typically have a critical incident heat flux associated with ignition, such that exposure to a heat flux below the critical heat flux will not result in ignition. Since the stagnation point heat fluxes from these nozzles is generally decreasing with increasing height, if a critical ignition flux is known, a critical height can be determined from Figure 21, such that no ignition will occur above that height for a specific material. This critical height can be used as a performance characteristic of unwanted ignition propensity. The cigarette lighter

nozzle with the lower values of  $(\dot{q}_0'')_{\max}$  will have better unwanted ignition propensity than the others using only information about the heat flux as a comparison assuming that the stagnation point heat flux is more important than the average value. Based on the data, the Diffusion nozzle produces the lower  $(\dot{q}_0'')_{\max}$  in the near field. However, the data for Premixed1 illustrates lower stagnation point heat fluxes in the far field, illustrating that Premixed1 will have better unwanted ignition propensity than the other two nozzles sufficiently far away from the source. Premixed1 produces better performance compared to Premixed owing to the energy loss to the combustion chamber and flame stabilizer as described in Section 3.1.2. Each of these nozzles demonstrate heat fluxes above the critical value for ignition of filter paper discussed below, and thus pose an unwanted ignition hazard.

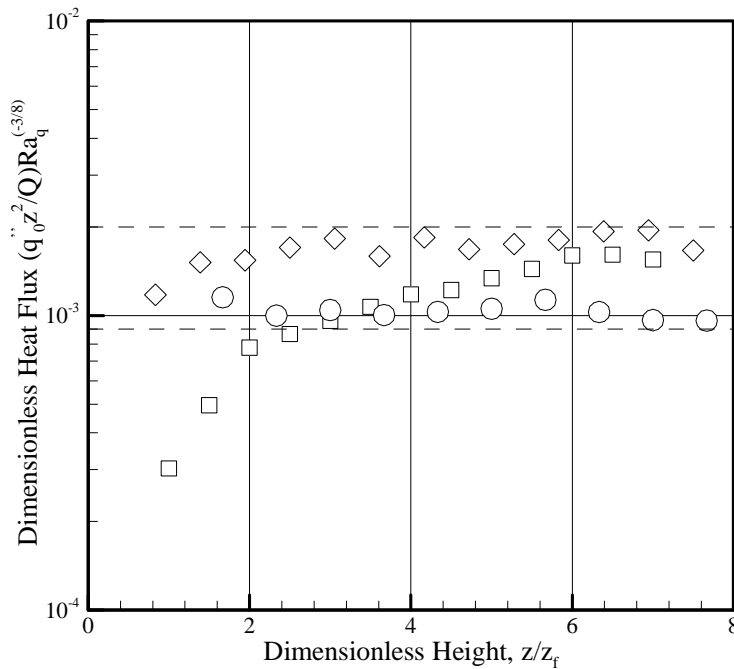


Figure 22: Scaling analysis of stagnation point heat flux assuming laminar flow and laminar stagnation point theory illustrating order of magnitude agreement.  
 □ - Diffusion    ○ - Premixed1    ◇ - Premixed2

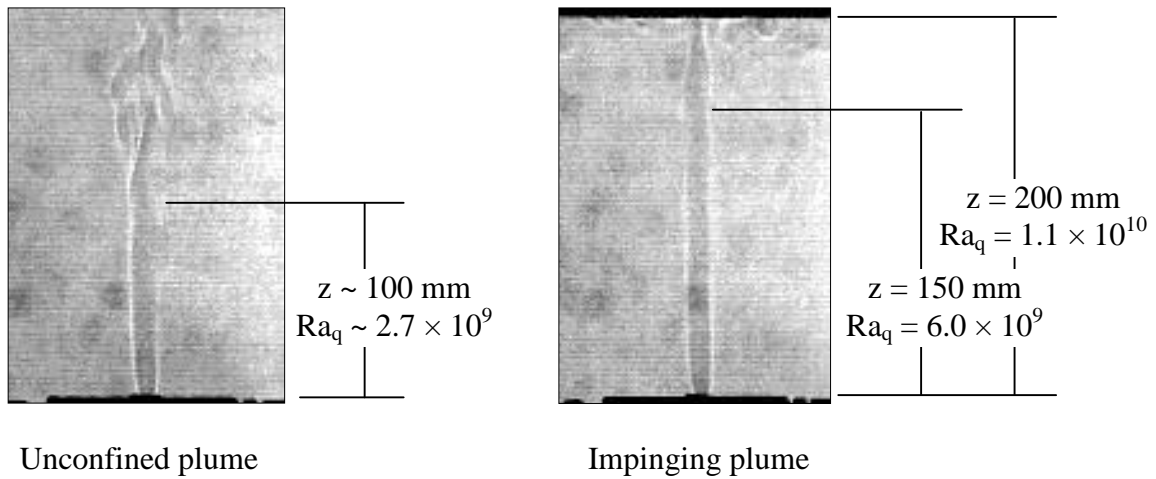


Figure 23: Sample plume shadowgraphs indicating a delayed turbulent transition in the impinging plume configuration. The turbulent transition occurs at the maximum sampling height observed in this study, and the turbulent transition in the impinging plume case is approaching the critical laminar condition at  $Ra_q < 10^{10}$  as prescribed by Bejan.<sup>23</sup>

### 3.1.4 Unwanted Ignition

An ignition test was designed in a simple configuration to evaluate the unwanted ignition propensity in a controlled environment. This test can also provide a validation of the heat flux measurements by showing that ignition time is consistent compared to the measured stagnation point heat flux at the same location while varying the cigarette lighter nozzle. A thin sheet of filter paper was oriented horizontally above the lighter. This orientation was the same as the thin copper plate such that the heat transfer to the filter paper would be analogous to that of the copper plate. Figure 24 illustrates the ignition data taken for the three existing nozzles. This data indicates critical ignition heights for the filter paper. The maximum heights of ignition were,  $h = 5.5$  cm for Diffusion,  $h = 6.1$  cm for Premixed1, and  $h = 9.6$  cm for Premixed2. Using an energy balance method assuming lumped heat capacitance

as illustrated in Equation (4), there is a direct association between time to ignition and incident heat flux. Figure 25 illustrates ignition time versus the observed stagnation point heat flux corresponding to the height of the test. This indicates good agreement between ignition time and stagnation point heat flux, and it also indicates an apparent critical heat flux of  $(\dot{q}_{ig}'' )_{crit} = 50 \text{ kW/m}^2$  as illustrated by the dashed line in Figure 25.

Scaling analysis can be performed on Equation (4). Nelson et al. found that the reciprocal of dimensionless ignition time is directly proportional to the incident heat flux assuming that the ignition temperature of the material is constant. They define dimensionless temperature as:

$$t^* = \frac{t_{ig} h_c}{(\tau \rho c)}, \quad (27)$$

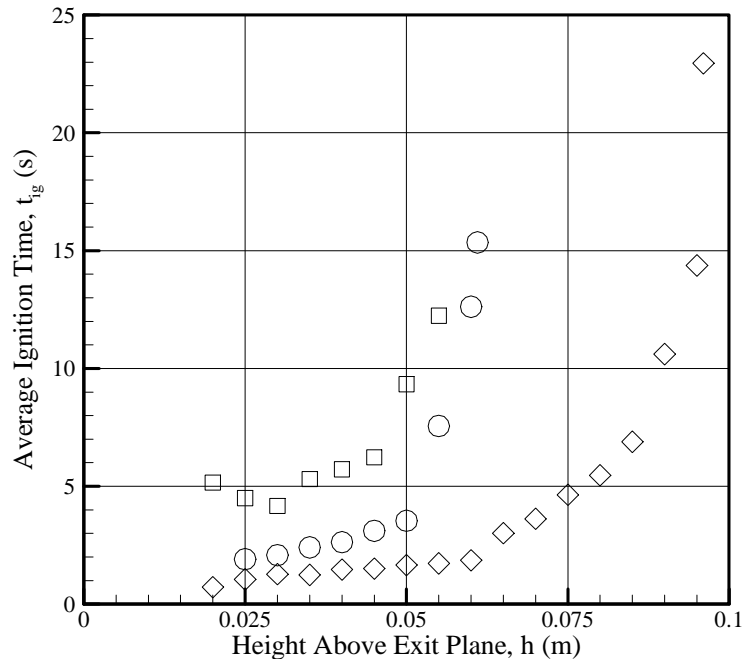


Figure 24: Ignition data for the three existing nozzles indicating a critical ignition height  $(h_{ig})_{crit}$  for each of the nozzles.

□ - Diffusion    ○ - Premixed1    ◇ - Premixed2

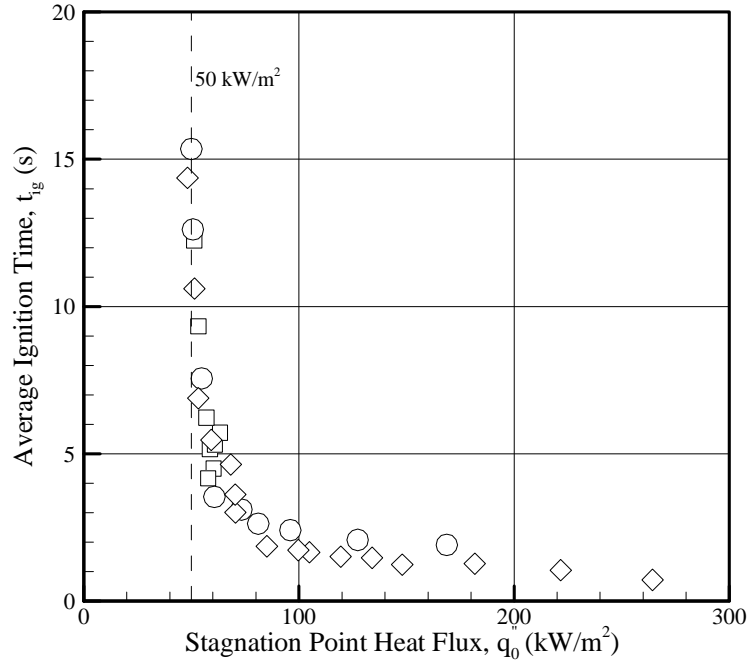


Figure 25: Ignition data versus stagnation point heat flux data, illustrating good agreement between ignition and heat flux information and a critical ignition heat flux  $(\dot{q}_{ig}'' )_{crit}$  as indicated by the dashed line at  $50 \text{ kW/m}^2$ .

□ - Diffusion    ○ - Premixed1    ◇ - Premixed2

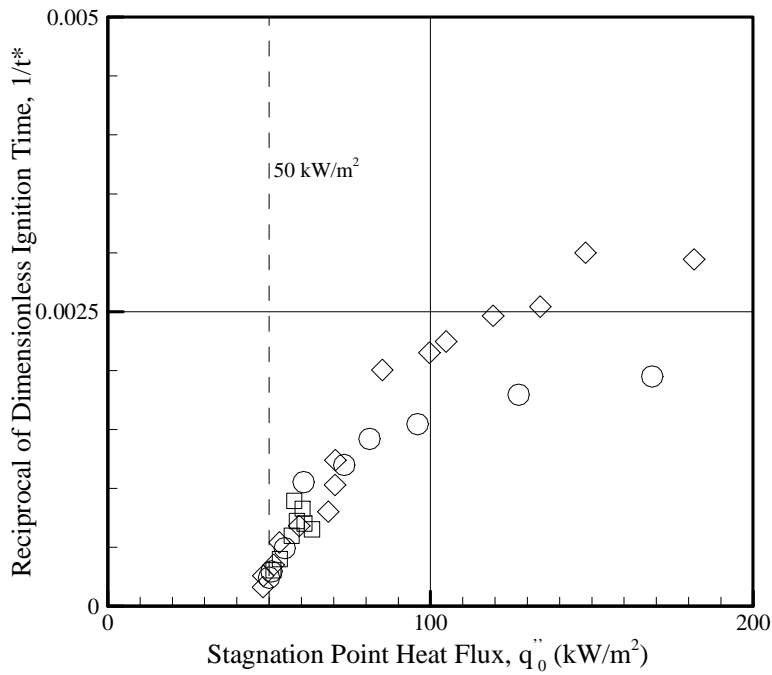


Figure 26: Scaling of ignition data indicating good agreement near the critical heat flux of  $(\dot{q}_{ig}'' )_{crit} = 50 \text{ kW/m}^2$ .

□ - Diffusion    ○ - Premixed1    ◇ - Premixed2

Where the convective heat transfer coefficient is assumed constant at  $h_c = 30 \text{ kW/m}^2\text{-K}$  as described by Nelson et al., and  $(\tau\rho c) = 111.9 \text{ J/m}^2\text{-K}$  for filter paper.<sup>20</sup> Figure 26 illustrates the results of this scaling method demonstrating excellent agreement near the critical ignition flux.

Now that a critical ignition flux has been obtained, the critical heat flux can be applied to the stagnation point heat flux profile in Figure 21 to determine a critical ignition height based on heat flux. From this information the critical ignition heights are,  $(h_{ig})_{crit} = 5.5 \text{ cm}$  for Diffusion,  $(h_{ig})_{crit} = 6.1 \text{ cm}$  for Premixed1, and  $(h_{ig})_{crit} = 9.6 \text{ cm}$  for Premixed2. These values agree with those reported in the data from Figure 24. Based on this information, the nozzle with the lowest value of  $(h_{ig})_{crit}$  will have better unwanted ignition propensity performance. Using this information, Diffusion produces the best performance. Premixed1 produces significantly better performance than Premixed2. This may be due to the energy transferred to the combustion chamber and flame stabilizer as described in section 3.1.2 or a difference in injection velocity which could change convective heat transfer or entrainment of the flow.

### **3.2 Development and Characterization of Prototype**

The purpose of developing this prototype nozzle is to evaluate the effectiveness of design modifications, which do not involve mechanical child safety features, on improving the unwanted ignition propensity performance of a cigarette lighter. Performance information from the three existing lighters, Table 2, was analyzed in order to determine a concept for the Prototype. The visible flame height, maximum heat flux, maximum centerline temperature, and ultimately the maximum

ignition height performance will all be targeted for deduction in the Prototype design. Among these characteristics, maximum heat flux is the most influential factor in predicting unwanted ignition propensity performance. Premixed1 demonstrates that each of these characteristics can be significantly reduced when the geometry of the nozzle dictates that the combustion chamber and flame stabilizer absorb some of the energy from the flame. Thus, a combustion chamber and flame stabilizer can be designed to completely contain the flame and maximize energy losses to the geometry. This must be done while accounting for geometry characteristics of cigarettes, and addressing the temperature rise of the nozzle.

The Prototype was designed following the concept of a combustion chamber into which a cigarette would be inserted for ignition. The flame stabilizer is needed to limit the insertion of the cigarette, because inserting the cigarette too close to the source will cause extinction of the flame. This combustion chamber and flame stabilizer will also act as a heat sink for the flame. The Prototype design approach utilized three, concentric, stainless steel tubes, where the inside diameter of the inner tube (Tube 1) was 9.65 mm, slightly greater than the diameter of a cigarette. Details of the Prototype design are illustrated in Figure 7 and Appendix B. Three tubes were selected because the outer tubes act as a radiation shield for the inner tube; effectively increasing the time over which the energy absorbed by the inner tube is released to the environment. This recession concept was successful in reducing all of the unwanted ignition hazard characteristics as will be illustrated by data taken from the Prototype. Scaling of data from the Prototype will not be performed in most cases because the design introduces too many factors that can influence its behavior.

The Prototype nozzle was evaluated for using the same technique described for the existing nozzles. However, since the steady state condition of the Prototype occurred when the three tubes were heated to a steady state temperature, the temperature and heat flux measurements are not completely representative of the actual conditions of use. Reasonably, the steady state condition of the Prototype is more indicative of an absolute worst-case scenario. Typically, the values measured for temperature and heat flux will be higher than at the initial condition; however the steady state experiments still provide a conservative estimate of the actual performance.

### **3.2.1 Prototype Flame Height**

The combustion chamber of the Prototype nozzle was designed to completely contain the flame. This resulted in a condition where there was no visible flame. This is a very beneficial condition, because the peak temperatures observed in the three existing lighters all occurred within the flame. The ‘invisible’ flame condition also precludes scaling of the Prototype heat flux data because of difficulties in determining  $z_f$ .

### **3.2.2 Prototype Temperature**

The radiation corrected temperature results for the Prototype illustrate significant near field improvement over the performance of the three existing nozzles. The maximum observed temperature for the Prototype is 1095 K at  $h = 2.0$  mm. This is a temperature reduction of 928 K below the existing Premixed2 maximum

Table 2: Existing Cigarette Lighter Hazard Characteristics.

Lighter Label	Visible Flame Height, $h_f$ (mm)	Maximum Heat Flux, $(\dot{q}_o'')_{\max}$ (kW/m <sup>2</sup> )	Maximum Temperature, $T_{\max}$ (K)	Maximum Ignition Height, $(h_{ig})_{\max}$ (cm)
Diffusion	20	63	1930	5.5
Premixed1	9	169	1763	6.1
Premixed2	15	326	2022	9.6

temperature (Prototype uses the same fuel nozzle as Premixed2). Clearly, the amount of energy transferred to the combustion chamber and flame stabilizer is significant. While the near field temperature is greatly reduced, the far field temperature is not significantly reduced. This may result from a delayed turbulent transition compared to the existing nozzles. This delayed turbulent transition can be explained using  $Ra_q$  where a reduced effective energy release rate,  $\dot{Q}$ , is used. This energy reduction is due to heat absorption by the combustion chamber and flame stabilizer. A reduction in the effective energy release rate will cause a proportional reduction in  $Ra_q$  causing a delayed turbulent transition.

A temperature scaling analysis can roughly be performed on the Prototype data however, it does not account for an effective reduction in  $\dot{Q}$  such that  $z^*$  is defined in the same way for the Prototype as it is for the existing nozzles. This analysis the  $z_0 = 0$  assumption is no longer valid. The introduction of the tube causes a virtual origin based on reduced entrainment when the flow is still in the tube. Thus the virtual origin should be approximately equal to the recession depth  $(\delta_{light})_{Prototype} =$

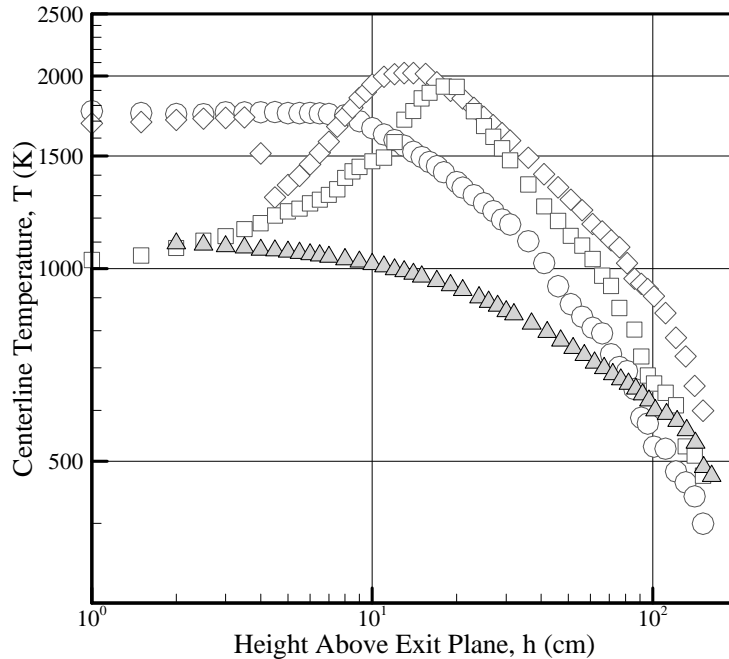


Figure 27: Centerline temperatures of all tested nozzles indicating that the temperature of the Prototype near the exit plane is much lower than those observed for the existing nozzles.

□ - Diffusion    ○ - Premixed1    ◇ - Premixed2    ▲ - Prototype

79 mm because that is the height at which air can be freely entrained. A virtual origin was determined for the Prototype by matching the far field temperature decay to the  $(-5/3)$  power law decay observed for plumes. This method resulted in  $(z_0)_{Prototype} = 85$  mm, which is conceptually correct because the flow propagating from a tube is not expected to behave as a plume initially. The finite area of the tube and the finite velocity of the flow at the exit plane will dictate that entrainment does not follow plume behavior for some distance above the exit plane. The results of this scaling analysis are illustrated in Figure 28. According to this information, fully established turbulent flow occurs at  $z^* \sim 6$  which is greater than that of the existing nozzles. Temperature fluctuations also indicate a delay in the turbulent transition at  $z^* \sim 4$  as illustrated in Figure 29.

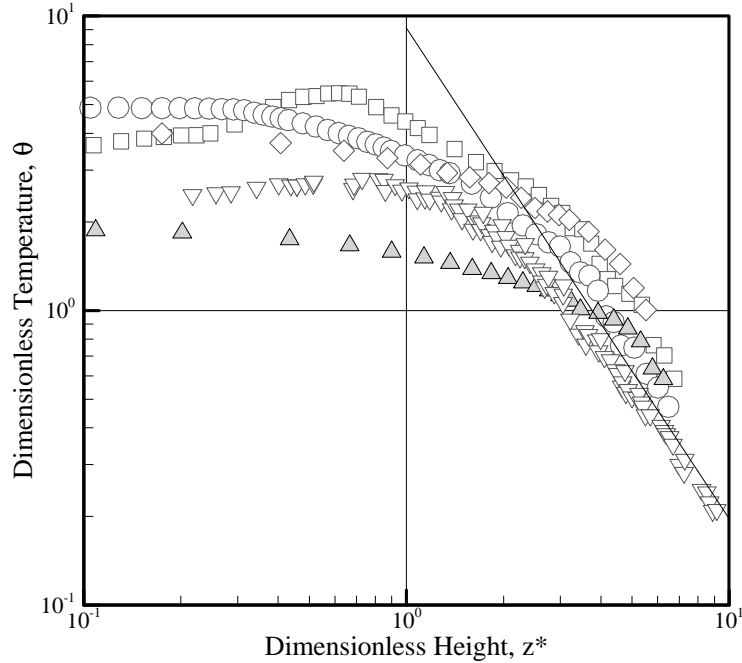


Figure 28: Scaling analysis of all tested nozzles compared to data taken by McCaffrey and a correlation by Heskestad, indicating that turbulent plume behavior for the Prototype nozzle occurs at a higher  $z^*$  than the existing nozzles.<sup>30</sup>

□ - Diffusion   ○ - Premixed1   ◇ - Premixed2   ▲ - Prototype   ▽ - McCaffrey  
 — - Heskestad

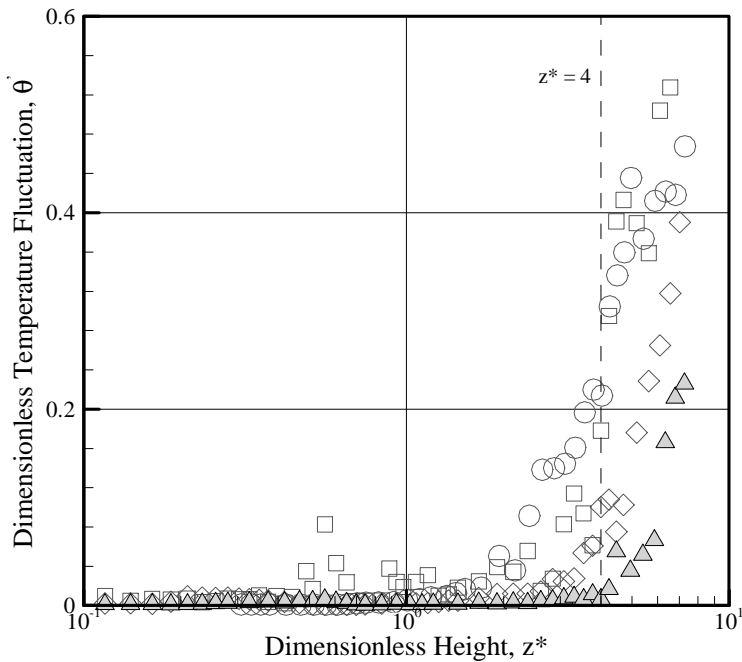


Figure 29: Temperature fluctuations of all tested nozzles where the turbulent transition region for the existing nozzles is  $z^* \sim 2-3$ , indicating a delayed turbulent transition for the Prototype at  $z^* \sim 4$ .

□ - Diffusion   ○ - Premixed1   ◇ - Premixed2   ▲ - Prototype

### 3.2.3 Prototype Surface Temperature

Surface temperatures of the Prototype are a significant factor describing its performance and its commercial viability. If the surface temperature of the nozzle increases rapidly to the threshold of pain or even high enough to cause ignition of nearby materials, its unwanted ignition propensity performance will be suspect. A simple heat transfer analysis was performed using a two-zone approach based on thermal resistance methods. A two-zone approach was used to account for the temperature difference along the length of each tube as illustrated by the data in Figures 30 to 32. Each tube was split into two zones at the height of the flame stabilizer. The resistance analog was applied to the concentric radial tube configuration of the Prototype lighter. The effects of radiation and natural convection were evaluated for each zone based on simple correlation using a first order approximation of Fourier's Law, Newton's Law of cooling and the Stefan-Boltzmann Law presented by Incropera.<sup>26</sup> Zone wise energy balance equations are presented below where  $j = 1$  or  $2$  corresponding to the bottom zone and the top zone respectively.

③ Tube 1 (inner tube)

$$mc_p \frac{\Delta T}{\Delta t} = S_j X \dot{Q} + (-1)^j \dot{q}_{cond} - (\dot{q}_{rad})_{net,1-2} - \dot{q}_{conv}, \quad (28)$$

③ Tube 2 (middle tube)

$$mc_p \frac{\Delta T}{\Delta t} = (\dot{q}_{rad})_{net,1-2} + (-1)^j \dot{q}_{cond} - (\dot{q}_{rad})_{net,2-3} - \dot{q}_{conv}, \quad (29)$$

③ Tube 3 (outer tube)

$$mc_p \frac{\Delta T}{\Delta t} = (\dot{q}_{rad})_{net,2-3} + (-1)^j \dot{q}_{cond} - (\dot{q}_{rad})_{net,3-\infty} - \dot{q}_{conv}, \quad (30)$$

The details of the heat transfer analog equations and the method for solving the problem are illustrated in Appendix E. The model was also designed to resolve temperature performance after the nozzle was shut off. This was necessary to investigate the surface temperature increase of the outer tubes after the nozzle is shut off due continued heating from the inner tube, which is at a higher temperature.

In testing an un-cooled Prototype, a natural cutoff time occurred regularly at 110 s. This natural cutoff time was a result of extreme heating and thermal expansion of the orifice such that the fuel flow was reduced to the point of extinction. Therefore data was taken for the nozzle while the nozzle was shut off at  $t = 110$  s and the model predictions were calculated using the same cutoff time. The results of the model temperature predictions are illustrated along surface temperature measurements taken with a similar shutoff time in Figure 31 to 33 for each tube. A legend is provided in Figure 30 illustrating the locations of thermocouples and zones. The model illustrates reasonably accurate predictions of surface temperature for all tubes when the model inputs were set to known values for stainless steel. The key inputs for the model included the physical, thermal and geometric properties of all three tubes, a shutoff time, a time step, the total energy release rate of the flame, and an approximation of the fraction of energy transferred from the flame to tube 1. The only input requiring engineering judgment is the fraction of energy transferred from the flame to tube 1. This value was approximated qualitatively by matching the results of the tube 1 surface temperature calculations to the data taken for tube 1. Input values for the model are illustrated in Appendix E.

This model can also be used in predicting surface temperature performance differences when the construction material properties are changed. Sensitivity analysis of the model for designs of similar geometry shows that material with high density, high specific heat and low emissivity illustrate improved performance. Polished stainless steel appears to have been a good selection of material, because it has a high density, high specific heat and a low emissivity. The three-tube configuration also demonstrates a dramatic surface temperature improvement over the two-tube configuration.

The peak exposed surface temperature of the Prototype also has better performance in comparison to that of Premixed1 for similar operation time, as illustrated in Figure 34. The peak exposed temperature of the Prototype is 344 K at  $t = 379.5$  s and the peak exposed temperature for Premixed1 is 453 K at  $t = 110$  s. In fact, the performance of Tube 2 (middle tube) is better than Premixed1. Depending on the level of safety desired a two-tube design might be determined as sufficiently safe.

### **3.2.4 Prototype Heat Flux**

The heat flux measurements for the Prototype design demonstrate a dramatic improvement over the existing nozzles. The maximum observed heat flux was  $(\dot{q}_o'')_{\max} = 51 \text{ kW/m}^2$  at  $h = 2$  mm. The radial heat flux profile corresponding to the peak observed heat flux for all of the lighters is illustrated in Figure 34. The stagnation point heat flux versus height is illustrated in Figure 35 for all lighters. The data for the Prototype is indicative of the worst-case scenario. In actual use, the

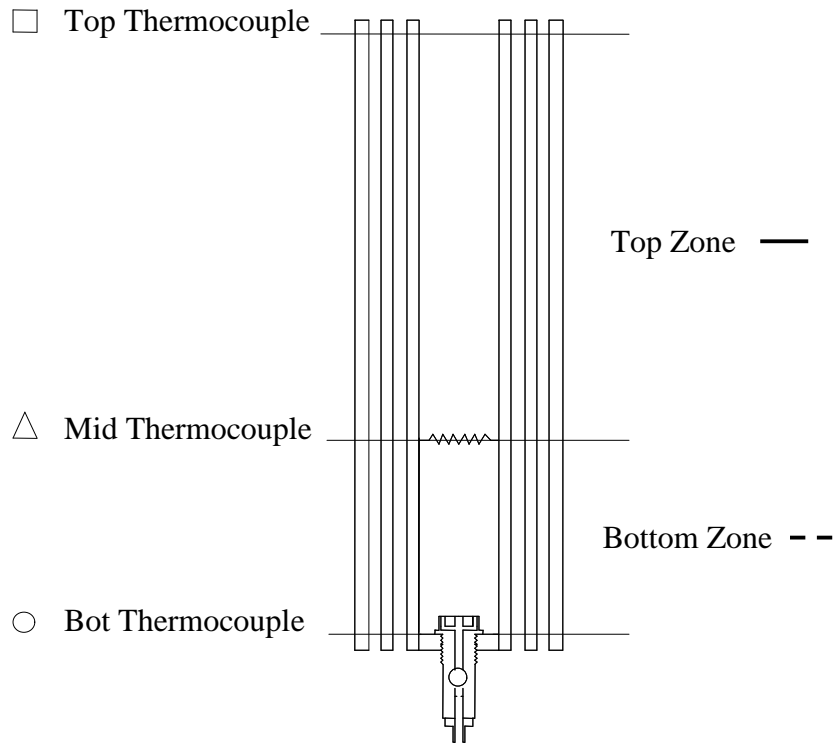


Figure 30: Legend for Figures 31 to 33.

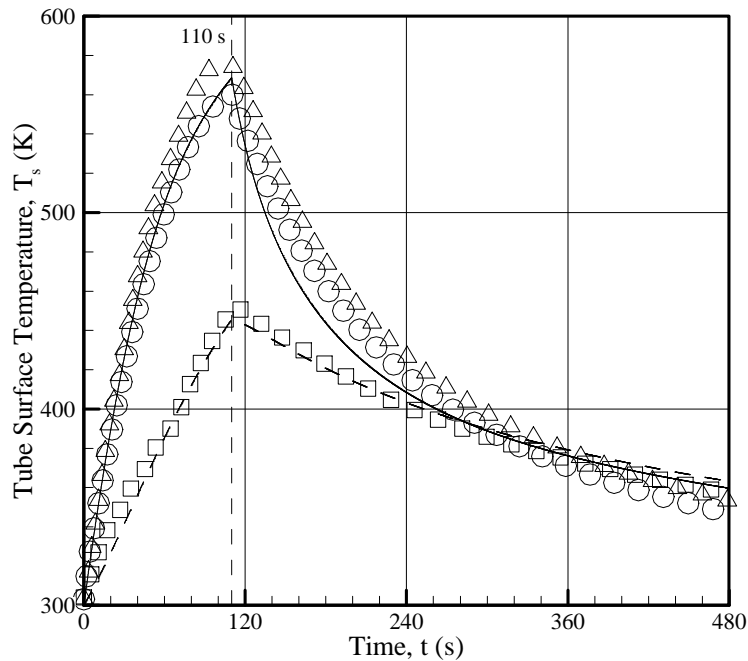


Figure 31: Tube 1 (inner tube) surface temperatures, the fraction of energy transferred to tube 1 was the only unknown input for the model, therefore its value was modified to make the surface temperatures at  $t = 110$  s match the data taken for a similar cutoff time.

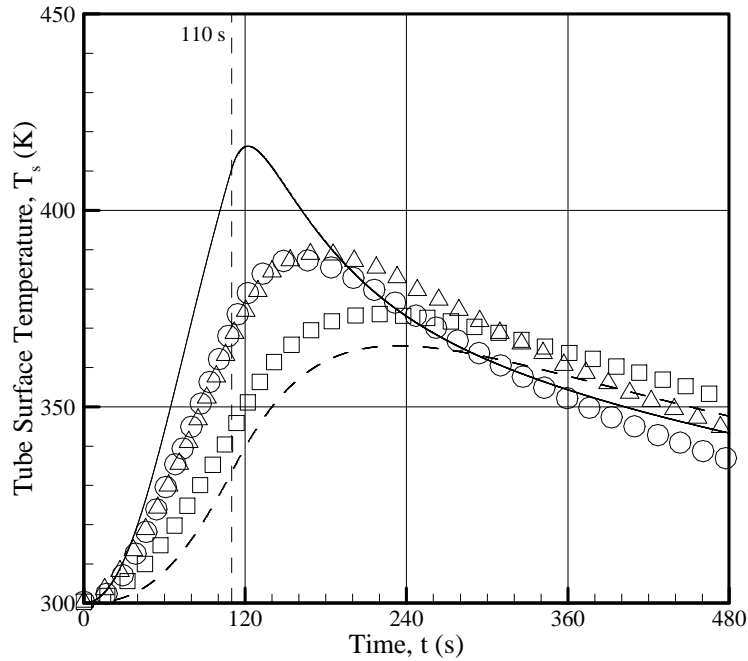


Figure 32: Tube 2 (middle tube) surface temperatures, illustrating similar surface temperature behavior predicted by the analysis compared to that observed in the data.

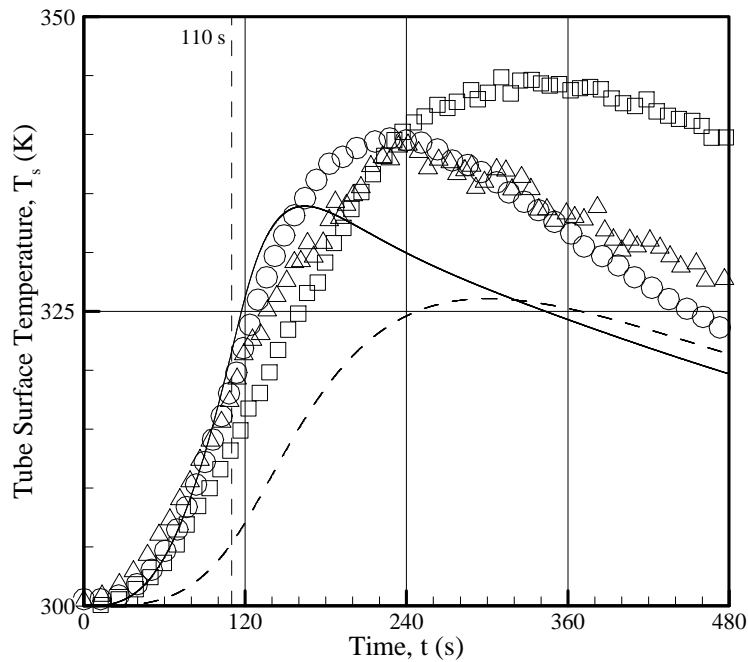


Figure 33: Tube 3 (outer tube) surface temperatures, illustrating similar surface temperature behavior predicted by the analysis compared to that observed in the data.

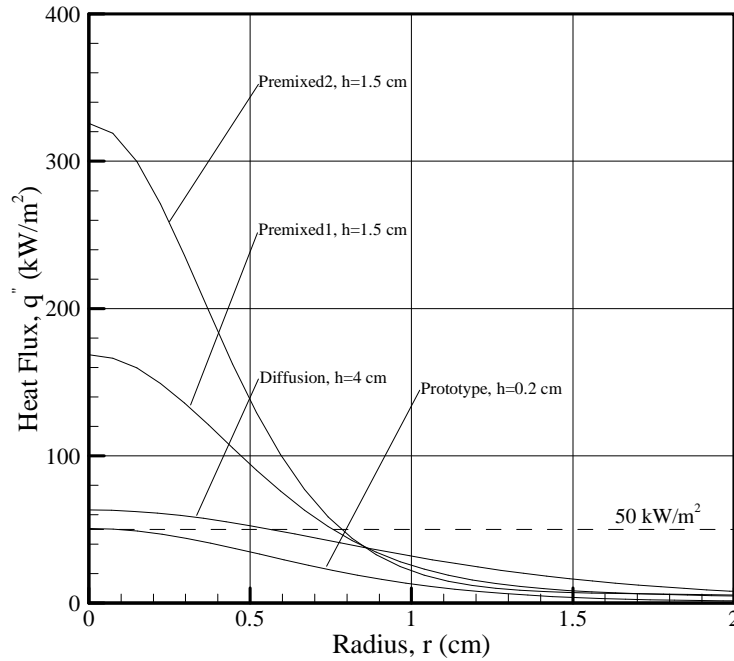


Figure 34: Radial heat flux profiles corresponding to the peak observed stagnation point heat flux for all nozzles.

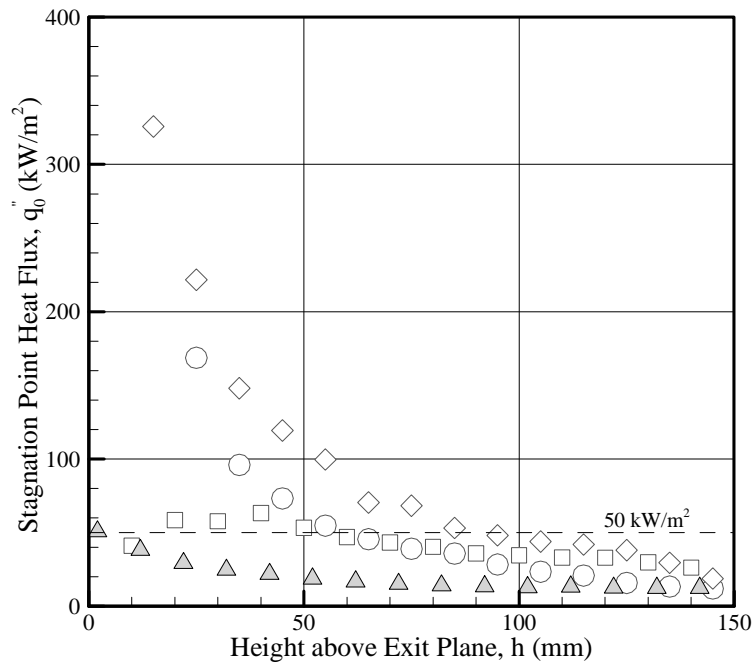


Figure 35: Stagnation point heat fluxes versus height for all nozzles tested indicating significant improvement of the Prototype over all other nozzles.

□ - Diffusion   ○ - Premixed1   ◇ - Premixed2   ▲ - Prototype

unwanted ignition propensity performance will be lower than the values reported for nearly all instances of operation. Scaling of the heat flux information for the Prototype is impossible because of the difficulties in measuring  $z_f$ .

### **3.2.5 Prototype Unwanted Ignition**

The results of several ignition test trials with the prototype nozzle, no flaming ignition was observed. Only a few tests resulted in any visible smoldering of the filter paper, while many tests at the same height illustrated no visible ignition. Therefore ignition testing of the Prototype nozzle illustrated no significant ignition time.

## **Chapter 4: Conclusions**

This study illustrates a detailed investigation into the ignition propensity of small flames such as cigarette lighters. The objectives of this study were to characterize ignition propensity of conventional cigarette lighters, and to create a concept that will demonstrate an improvement in unwanted ignition propensity from a cigarette lighter without adding mechanical child safety features. An experimental facility was designed and constructed to characterize centerline temperatures, heat flux to a horizontal flat plate, and ignition of filter paper in order to investigate the ignition propensity of flames from these lighters. Innovative diagnostics were employed to account for the scale of the experiment without sacrificing accuracy. A concept cigarette lighter was designed based on characteristics of existing cigarette lighters that demonstrated improved ignition propensity or need for improvement. The concept was tested using the same methodology developed for the existing cigarette lighters. The results of the investigation illustrate many interesting behavior of each lighter tested.

### **4.1 Temperature Measurements**

Laminar flames, such as those produced by cigarette lighters can produce dramatically different centerline temperature profiles within the flame. The peak temperatures of these laminar flames can vary widely based on fuel-air mixing and energy losses to the combustion chamber. Diffusion flames and premixed flames that do not have energy losses illustrate maximum temperatures near the adiabatic flame temperature for the fuel. Centerline temperatures observed sufficiently far away from

the source decay similarly to turbulent plume scaling and data taken by McCaffrey.<sup>6</sup> Temperature fluctuations indicate that turbulence levels dramatically increase at the height where turbulent plume scaling behavior is observed. The turbulent transition agrees to within an order of magnitude of the maximum turbulent transition height where  $Ra_q = 10^{10}$  as prescribed by Bejan.<sup>23</sup> In the laminar region, temperature decay is difficult to scale because of variations in mass, momentum and buoyancy flux as discussed by Morton.<sup>8</sup>

Centerline temperature profiles, however, are a weak indicator of ignition propensity performance. The most significant parameter for determining ignition propensity from centerline temperature profiles is the peak temperature. Turbulent transition is only significant in scaling of the data, and does not provide a significant impact on ignition propensity. Results from the Prototype demonstrate that the peak centerline temperature can be significantly reduced with a simple modification of the combustion chamber and flame stabilizer.

## **4.2 Heat Flux Measurements**

The stagnation point heat fluxes observed in this study illustrate extremely high local heat transfer. Maximum values reported by Veldman et al. are on the order of  $1 \text{ kW/m}^2$  at the stagnation point for fires having energy release rates of 1.17 kW to 1.53 kW.<sup>10</sup> Faeth and You have reported maximum values for stagnation point heat fluxes of  $8 \text{ kW/m}^2$  to  $12 \text{ kW/m}^2$  for fires having energy release rates of 1.67 kW and 8.51 kW respectively.<sup>11</sup> This study reports peak stagnation point heat fluxes of  $51 \text{ kW/m}^2$  to  $326 \text{ kW/m}^2$  for 75 W flames. Clearly the local heat loading from these

small flames is significantly higher, one to two orders of magnitude, than that for a larger flame. It also illustrates that flames having the same energy release rate can produce dramatically different heat loadings based on different nozzle geometry. Scaling of the heat fluxes illustrates very little scaling agreement with traditional scaling methods. A laminar scaling term was developed to produce better correlation, resulting in an order of magnitude agreement as illustrated in Figure 22. The study performed by Kokkala shows that heat flux scaling is only accurate to an order of magnitude.<sup>28</sup> More research is needed to validate the scaling methods for heat flux.

Practically, heat flux measurements are the strongest indicator for ignition propensity performance. Ignition time is dependent on incident heat flux, and the material properties. The peak incident heat flux is an indicator of the various types of materials that can be ignited, while the heat flux versus height profile can indicate a region of the plume in which a particular material can be ignited. These two parameters can be used in a comparison of ignition propensity performance. Results from the Prototype illustrate that both peak incident heat flux and the ignition region of a cigarette lighter can be significantly reduced by a simple modification of the combustion chamber and flame stabilizer of the nozzle.

#### **4.3 Ignition of Filter Paper Measurements**

Simple ignition testing demonstrates that the method used to determine the incident heat flux produces consistent results for all the cigarette nozzles tested. Ignition time and incident stagnation point heat flux measurements were directly correlated to find a critical ignition heat flux for filter paper of  $50 \text{ kW/m}^2$ . This

information allowed for a determination of a specific region of the plume where each lighter produced ignition of the filter paper. This region provides a specific example for comparison of the cigarette lighters. Results from the Prototype illustrate that the region of ignition for filter paper can be effectively reduced to zero by a simple modification of the combustion chamber and flame stabilizer.

#### **4.4 Overall Prototype Performance**

A simple comparison of the critical parameters describing ignition propensity illustrates that the Prototype concept successfully improves unwanted ignition propensity performance when compared to existing cigarette lighter designs. The hazard parameters for all four tested nozzles are listed in Table 3. The Prototype demonstrates significant reduction in flame height, peak centerline temperature, maximum observed incident heat flux, and critical ignition region. Actual performance improvements are:

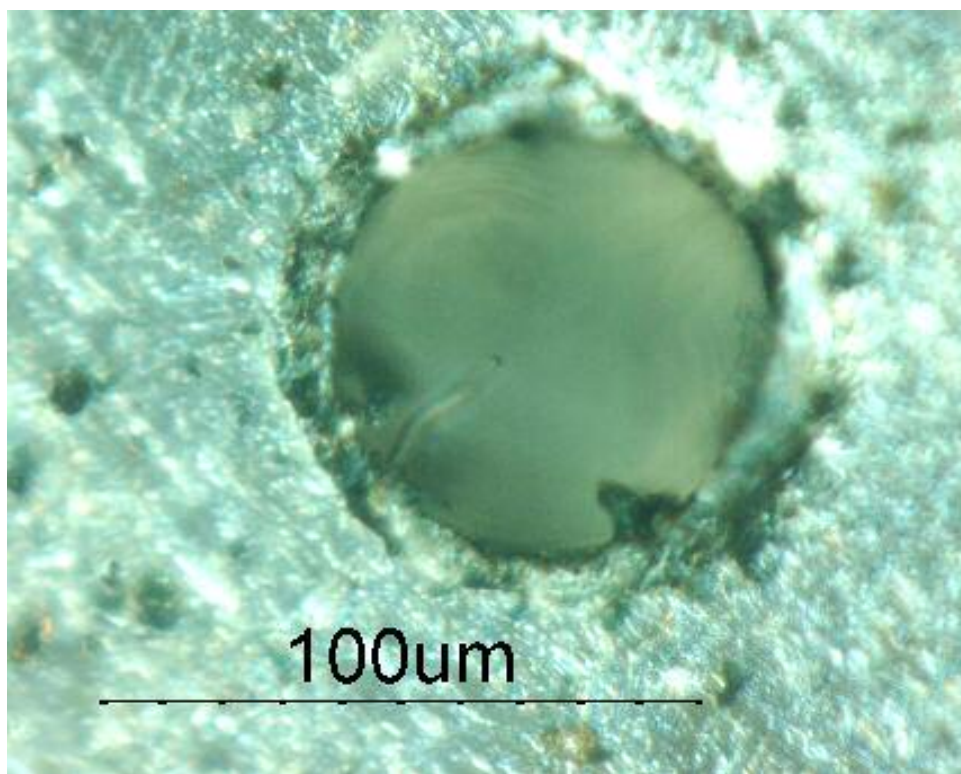
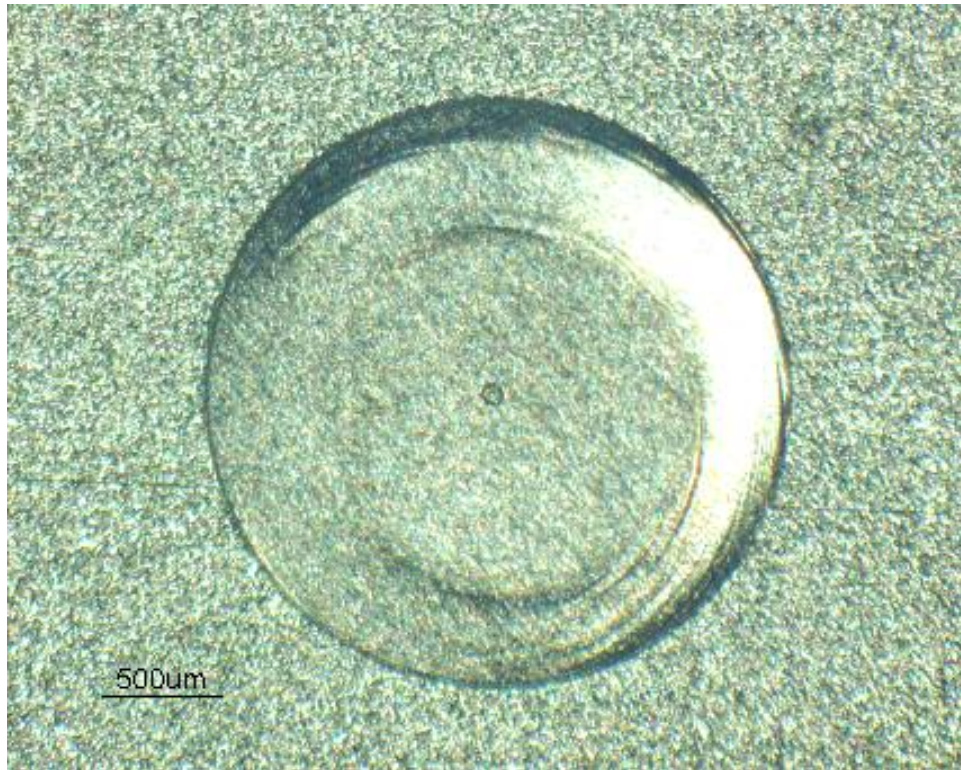
- visible flame height is reduced to zero,
- peak centerline temperature is reduced by 836 K, 668 K, and 928 K for Diffusion, Premixed1, and Premixed2 respectively,
- maximum observed heat flux is reduced by a factor of 1.24, 3.23, and 6.42 from Diffusion, Premixed1, and Premixed2 respectively,
- critical ignition height for filter paper is reduced effectively to zero because ignition tests demonstrated insignificant information.

Table 3: Hazard characteristics for all nozzles tested

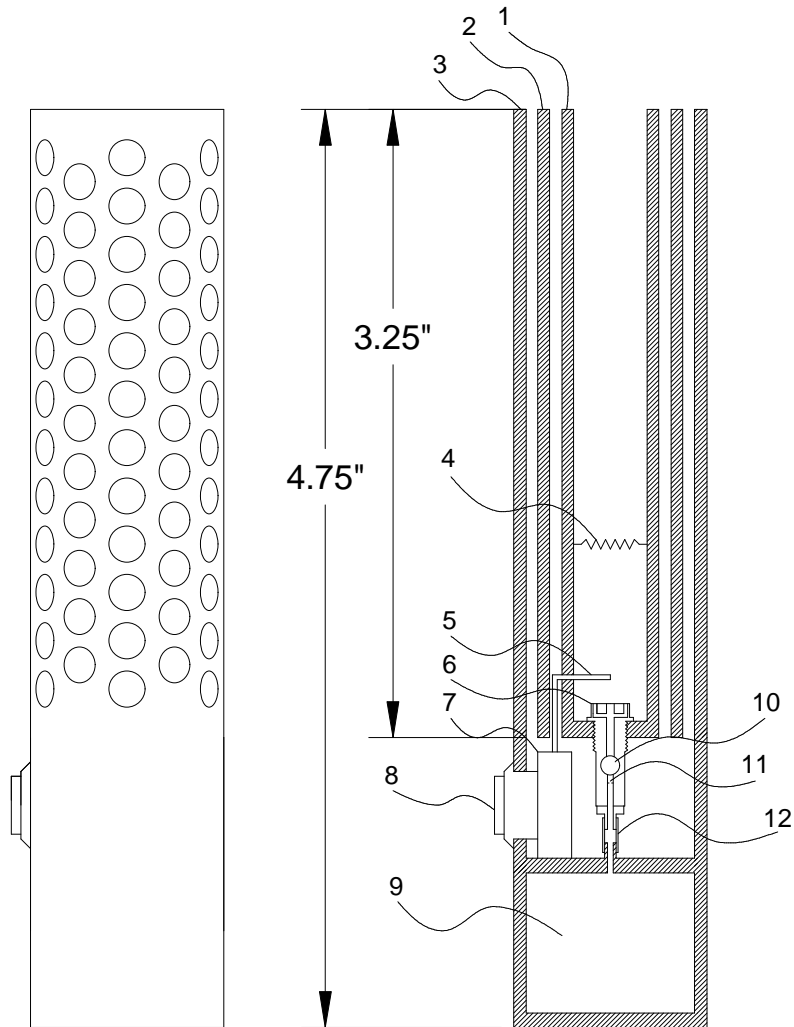
Lighter Label	Visible Flame Height, $h_f$ (mm)	Maximum Heat Flux, $(\dot{q}_o'')_{\max}$ (kW/m <sup>2</sup> )	Maximum Temperature, $T_{\max}$ (K)	Maximum Ignition Height, $(h_{ig})_{\max}$ (cm)
Diffusion	20	63	1930.1	5.5
Premixed1	9	169	1762.5	6.1
Premixed2	15	326	2022.1	9.6
Prototype	0	51	1094.5	0

The performance caveat of the Prototype is the exposed surface temperature of the nozzle. This caveat can be resolved by selecting materials with high density, high specific heat and low surface emissivity as well as by increasing the number of concentric tubes in the design. The design selected illustrates lower exposed surface temperatures than those observed for Premixed1 demonstrating an acceptable performance level for commercial viability. The Prototype also has sufficient heating capacity to ignite a cigarette when the cigarette is inserted into the combustion chamber to the flame stabilizer. Overall, the Prototype illustrates an effective concept in reducing the unwanted ignition propensity of cigarette lighters without introducing mechanical child safety features.

**Appendix A: Illustration of Fuel Orifice in Premixed1, Premixed2  
and Prototype**



## Appendix B: Proposed Cigarette Lighter Design Utilizing the Prototype Concept



1. Tube 1 (inner tube), Inside Diameter: 0.38 in, Outside Diameter: 0.5 in
2. Tube 2 (middle tube), Inside Diameter: 0.63 in, Outside Diameter: 0.75 in
3. Tube3 (outer tube), Inside Diameter: 0.87 in, Outside Diameter: 1 in
4. Titanium wire flame stabilizer
5. Spark ignition wire
6. Burner nozzle
7. Piezoelectric spark device
8. Operation button
9. Butane fuel reservoir
10. Air mixing chamber
11. Orifice (Appendix A)
12. Fuel connection tube

## Appendix C: Illustration of the National Instruments Program Diagram used for High Frequency Temperature Measurements

Program Window:

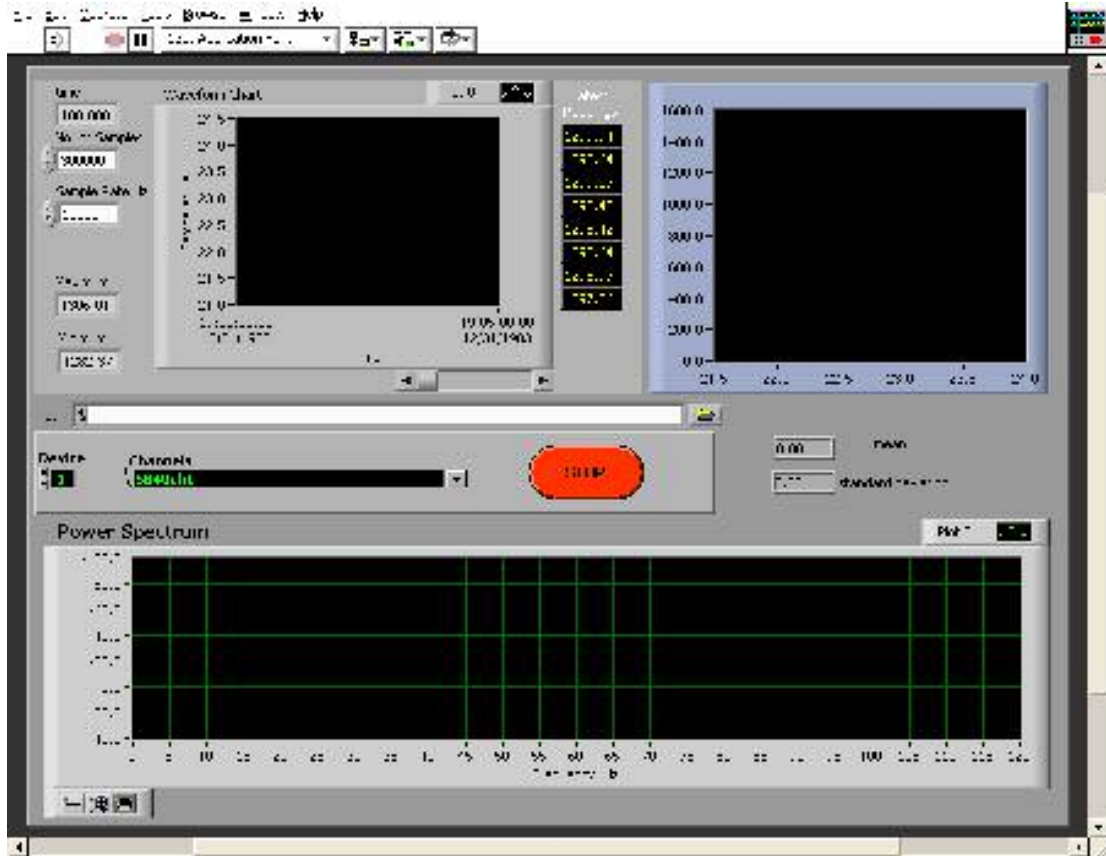
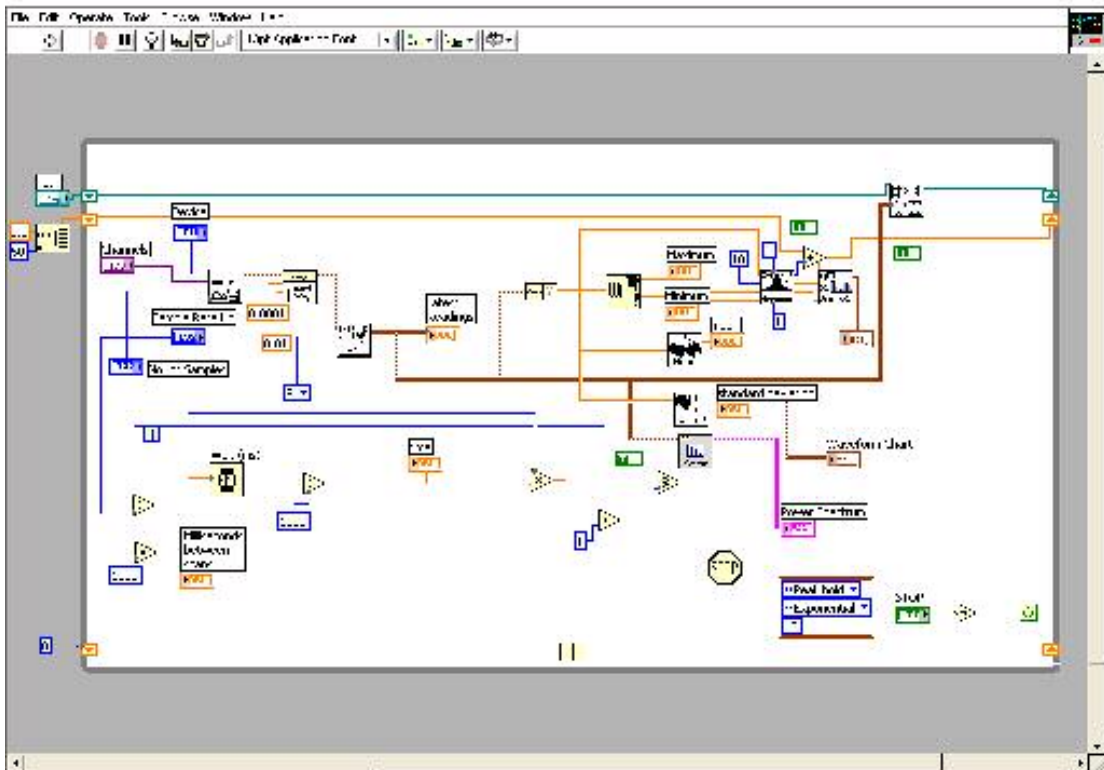


## Diagram Window:



## Appendix D: Matlab Program for Processing Heat Flux to a Horizontal Flat Plate

```
clc
clear all

% Input parameters

H = .15;           % Sampling traverse height, m
Ta = 300;          % Ambient temperature, K
dr = 0.000603125; % Pixel size, m
emiss = .95;       % Emissivity of flat plate
k = 386;           % Conductivity of flat plate, W/m-K
d = .000762;       % Thickness of flat plate, m
H = H - .005;      % Offset correction, m

% Image loading

start=1;
End=300;

average = zeros(240,320); % Creates a matrix of zeros

% Loads the image files and adds them all together

for k=start:End;
    str = int2str(k);
    file=['two_cm_',str,'] ;
    Mo=load (file) ;
    matlab= getfield(Mo,file);
    average=average+matlab;
end

% Divides the sum of all the images and divides by the number of images
% to get the mean temperature of any point

average=average./(End-start+1);

% Output results to file

save results.dat average -ascii

% Finds the location of the peak temperature at point [I,J]

[C,J]=max(max(average));
[C,I]=max(max(average,[],2));
```

```

% Best function constant parameters

m1 = 343.29
m2 = 7.5192e+05
m3 = -1.095e+07
m4 = 3.9334e+09
m5 = 2.4084e+13
m6 = 2248.7
m7 = 7.5308e+10

% Model for convective heat transfer coefficient

Tbar = mean(mean(average));
h = (9.81*(Tbar-
Ta)/(Ta*.00001589*.0000225)*(38.5*27/(38.5*2+27*2))^3)^(1/3)*.15*.0263/(38.5*
27/(38.5*2+27*2));

% Numerical evaluation

for m=1:115;

    % Spatial temperature average
    T_R1(m,1) = average(I,J+m-1);
    T_L1(m,1) = average(I,J-m+1);
    T_U1(m,1) = average(I+m-1,J);
    T_D1(m,1) = average(I-m+1,J);
    T_1(m,1) = (T_R1(m,1)+T_L1(m,1)+T_U1(m,1)+T_D1(m,1))/4;
    T_bar(m,1) = T_1(m,1);

    % Convection, W/m^2
    Q_h(m,1) = h*(T_bar(m,1)-Ta);

    % Radiation, W/m^2
    Q_r(m,1) = emiss*5.67*10^-8*(T_bar(m,1)^4 - Ta^4)*2;

    % Convection plus radiation, W/m^2
    Q_(m,1) = Q_h(m,1)+Q_r(m,1);
end

% Determination of r and R = r^2

r_1 = (0:m-1)*dr;
r = transpose(r_1);
for t=1:m
    R(t,1) = (r(t,1))^2;
end

```

```

% Evaluation of derivatives

for n=1:m;
    y(n,1) =
        (m1+m2*x2(n,1)+m3*x2(n,1)^2+m4*x2(n,1)^3+m5*x2(n,1)^4)/(1+m6
        *x2(n,1)+m7*x2(n,1)^4);

    dy(n,1) =
        (m2+2*m3*x2(n,1)+3*m4*x2(n,1)^2+4*m5*x2(n,1)^3)/(1+m6*x2(n,1)
        +m7*x2(n,1)^4)-
        (m1+m2*x2(n,1)+m3*x2(n,1)^2+m4*x2(n,1)^3+m5*x2(n,1)^4)/(1+m6
        *x2(n,1)+m7*x2(n,1)^4)^2*(m6+4*m7*x2(n,1)^3);

    dydy(n,1) =
        (2*m3+6*m4*x2(n,1)+12*m5*x2(n,1)^2)/(1+m6*x2(n,1)+m7*x2(n,1)^
        4)-
        2*(m2+2*m3*x2(n,1)+3*m4*x2(n,1)^2+4*m5*x2(n,1)^3)/(1+m6*x2(n,
        1)+m7*x2(n,1)^4)^2*(m6+4*m7*x2(n,1)^3)+2*(m1+m2*x2(n,1)+m3*
        x2(n,1)^2+m4*x2(n,1)^3+m5*x2(n,1)^4)/(1+m6*x2(n,1)+m7*x2(n,1)^
        4)^3*(m6+4*m7*x2(n,1)^3)^2-
        12*(m1+m2*x2(n,1)+m3*x2(n,1)^2+m4*x2(n,1)^3+m5*x2(n,1)^4)/(1+
        m6*x2(n,1)+m7*x2(n,1)^4)^2*m7*x2(n,1)^2;
end

% Net conduction, W/m^2

for n=1:m;
    dTp(n,1) = dy(n,1)*-4*k*d;
    dTdTp(n,1) = dydy(n,1)*R(n,1)*-4*k*d;
    Q_cp(n,1) = dTp(n,1)+dTdTp(n,1);
end

% Total heat flux

for g=1:m;
    Qp_flux(g,1) = Q_cp(g,1)+Q_r(g,1)+Q_h(g,1);
end

% Create output file

mat(:,1) = H; % Height of flat plate
mat(:,2) = r; % Radial position
mat(:,3) = Qp_flux; % Total heat flux at r
mat(:,4) = dr; % Pixel size
mat(:,5) = 2*pi*x*dr; % Differential area
mat(:,6) = 2*pi*dr*x.*Qp_flux; % Differential heat transfer

```

```
% Output to file
```

```
str1 = num2str(H);  
file1 = [str1, '_m.txt'];  
dlmwrite(file1,mat)
```

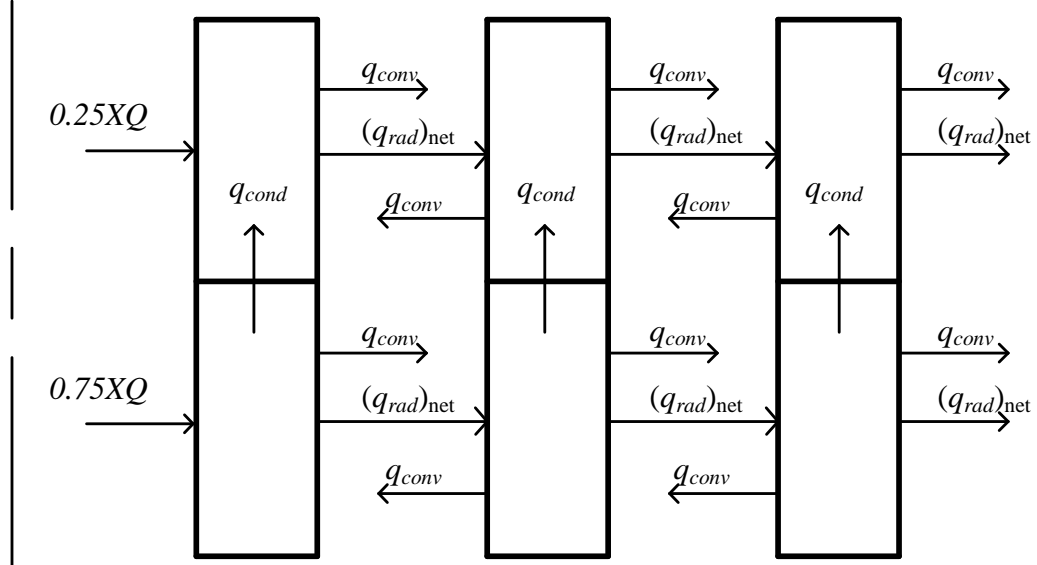
## Appendix E: Prototype Surface Temperature Prediction Method

**Inputs:**

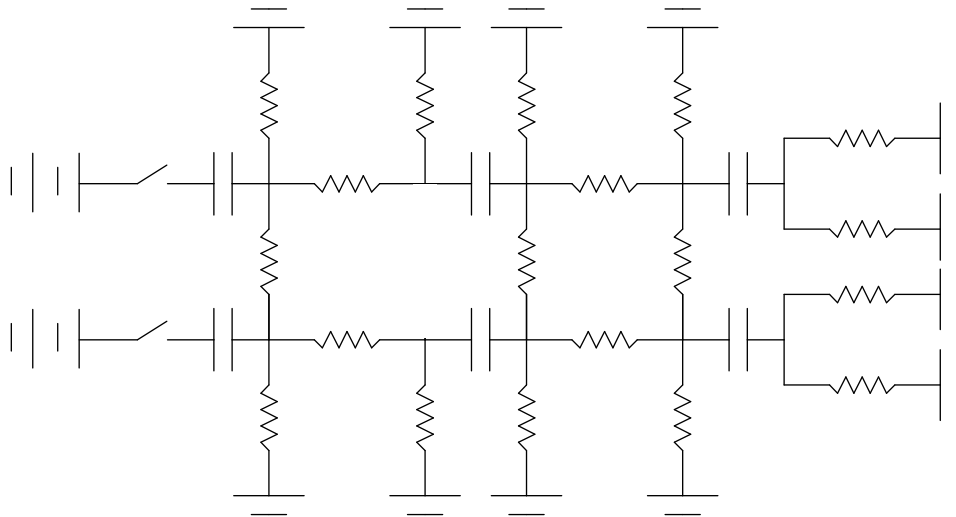
General Input Characteristics					
Fraction of Energy absorbed by Tube 1	Energy Release Rate, Q (W)	Ambient Temperature, T <sub>amb</sub> (C)	Shutoff time, t <sub>off</sub> (s)	Surface Emissivity, ε	Time Step, Δt (s)
0.5	75	23	110	0.18	0.1

Tube Input Characteristics					
Tube 1 (inner tube)		Tube 2 (middle tube)		Tube 3 (outer tube)	
ID (in)	0.38	ID (in)	0.63	ID (in)	0.87
OD (in)	0.5	OD (in)	0.75	OD (in)	1
L (in)	3.27	L (in)	3.27	L (in)	3.27
L <sub>zone1</sub> (in)	0.9	L <sub>zone1</sub> (in)	0.9	L <sub>zone1</sub> (in)	0.9
L <sub>zone2</sub> (in)	2.37	L <sub>zone2</sub> (in)	2.37	L <sub>zone2</sub> (in)	2.37
No. holes	132	No. holes	132	No. holes	132
No.zone1	30	No.zone1	30	No.zone1	30
No.zone2	102	No.zone2	102	No.zone2	102
hole dia. (in)	0.125	hole dia. (in)	0.125	hole dia. (in)	0.1875
ρ (kg/m <sup>3</sup> )	8238	ρ (kg/m <sup>3</sup> )	8238	ρ (kg/m <sup>3</sup> )	8238
c <sub>p</sub> (J/kg-K)	468	c <sub>p</sub> (J/kg-K)	468	c <sub>p</sub> (J/kg-K)	468
K (W/m-K)	13.4	k (W/m-K)	13.4	k (W/m-K)	13.4

**Diagram of heat transfer:**



**Analog resistance network (not labeled for the sake of simplicity)**



**Methods and equations:**

The model was solved numerically starting from the initial condition that all tubes were at ambient temperature. Energy balances were calculated iteratively by approximating the unknown surface temperature as the temperature calculated by the

previous time step using Equations (20) to (22). Temperature rises for each tube and time step were calculated starting at the inner tube, and stopping at the outer tube.

The energy transferred to tube 1 from the flame was approximated by

$$(q_{in})_j = S_j X \dot{Q}, \quad (31)$$

where  $X$  is the fraction of energy transferred from the flame to tube 1 and  $S_j$  is the fraction of energy transferred to zone  $j$  such that  $S_1 + S_2 = 1$  where  $S_1 = 0.75$  and  $S_2 = 0.25$  as an order of magnitude assumption. The natural convection was approximated by

$$q_{conv,i} = \frac{(T_i - T_\infty)}{R_{c,i}}, \quad (32)$$

where  $\dot{q}_c$  is the total energy transfer due to convection at a surface  $i$ ,  $T_i$  is the surface temperature of element  $i$ , and  $R_{c,i} = 1/h_c A_i$  such that  $h_c = 10 \text{ W/m}^2\text{-K}$  for natural convection flows and  $A_i$  is the surface area of surface  $i$ .<sup>26</sup> Radiation heat transfer was calculated by

$$(q_{rad})_{net,i \text{ to } i+1} = \frac{\sigma A_i (T_i^4 - T_{i+1}^4)}{R_i}, \quad (33)$$

where  $(\dot{q}_{rad})_{net,i \text{ to } i+1}$  is the net energy transfer between surface  $i$  and  $i+1$  due to radiation,  $\sigma$  is the Stefan-Boltzmann Constant, and

$$R_i = \frac{1}{\varepsilon} + \frac{1-\varepsilon}{\varepsilon} \left( \frac{r_i}{r_{i+1}} \right), \quad (34)$$

where  $\varepsilon$  is the surface emissivity and  $r_i$  is the radius of surface  $i$ . The radiation at the outer surface of tube three was calculated by

$$(q_{rad})_{net,3 \text{ to } \infty} = \varepsilon \sigma A_j (T_j^4 - T_\infty^4), \quad (35)$$

where the surroundings are assumed to be isothermal.<sup>26</sup> The two zones communicated through a simple first order conduction approximation

$$q_{cond} = \frac{kA_c}{L}(T_{bot} - T_{top}), \quad (36)$$

where  $q_{cond}$  is the total energy conducted from the bottom zone to the top zone,  $L$  is the distance between the geometric centers of the top and bottom zones,  $k$  is the thermal conductivity of the material, and  $A_c$  is the cross sectional area of the tube.

## Bibliography

- [1] Laitinen, D., "Candle Fires on the Rise," *NFPA Journal*, National Fire Protection Association, URL:  
<http://www.nfpa.org/Research/NFPAFactSheets/CandleSafety/CandleFiresOnTheRise/CandleFiresOnTheRise.asp>, Nov 2003.
- [2] Hall, J. R. Jr., *Children Playing with Fire*, National Fire Protection Association, June 2001.
- [3] *Juvenile Firesetter Intervention Research Project Final Report*, National Association of State Fire Marshalls, 2001.
- [4] *Annual Book of ASTM Standards*, "ASTM F400-00, Standard Consumer Safety Specification for Lighters", American Society for Testing and Materials, Philadelphia, 2003.
- [5] Morton, B. R., Taylor, G., and Turner, J. S., "Turbulent Gravitational Convection from Maintained and Instantaneous Sources," *Proceedings of the Royal Society of London, Series A*, Vol. 234, pp. 1-23, 1956.
- [6] McCaffrey, B. J., "Purely Buoyant Diffusion Flames: Some Experimental Results," Center for Fire Research, National Engineering Laboratory, *National Bureau of Standards*, No. NBSIR 79-1910, 1979.
- [7] Fujii, T. I., "Theory of Steady Laminar Natural Convection Above a Horizontal Line Heat Source and a Point Heat Source," *International Journal of Heat and Mass Transfer*, Vol. 6, pp. 597-606, 1963.
- [8] Morton, B. R., "Forced Plumes," Department of Mathematics, University of Manchester, pp. 151-163, 1958.
- [9] Alpert, R. L., "Fire Induced Turbulent Ceiling Jet," *Factory Mutual Research Corporation*, FMC 19722-2, 1971.
- [10] Veldman, C. C., Kubota, T., and Zukoski, E. E., "An Experimental Investigation of the Heat Transfer from a Buoyant Gas Plume to a Horizontal Ceiling – Part 1. Unobstructed Ceiling," Center for Fire Research, National Engineering Laboratory, *National Bureau of Standards*, No. NBS-GCR-77-97, 1975.
- [11] Faeth, G. M., and You, H. Z., "An Investigation of Fire Impingement on a Horizontal Ceiling," Center for Fire Research, National Engineering Laboratory, *National Bureau of Standards*, No. NBS-GCR-81-304 (1981).

- [12] Chow, W. K., "Numerical Studies on the Transient Behaviour of a Fire Plume and Ceiling Jet," *Mathematical and Computer Modelling*, Vol. 17, pp. 71-79, 1993.
- [13] Motevalli, V., "Numerical Prediction of Ceiling Jet Temperature Profiles During Ceiling Heating Using Empirical Velocity Profiles and Turbulent Continuity and Energy Equations," *Fire Safety Journal*, Vol. 22, pp. 125-144, 1994.
- [14] Motevalli, V., and Marks, C. H., "Transient and Steady State Study of Small-Scale, Fire-Induced Unconfined Ceiling Jets," *5<sup>th</sup> AIAA/ASME Thermophysical and Heat Transfer Conferences*, ed. Quintiere, J. G. and Cooper, L. Y., American Society of Mechanical Engineers, New York, pp. 49-61, 1990.
- [15] Drysdale, D. D., *An Introduction to Fire Dynamics, Second Edition, Ch. 6*, John Wiley and Sons, New York, pp. 193-232, 1998.
- [16] Zhou, Y. Y., Walther, D. C., and Fernandez-Pello, A. C., "Numerical Analysis of Piloted Ignition of Polymeric Materials," *Combustion and Flame*, Vol. 131, pp. 147-158, 2002.
- [17] Thomson, H. W., Drysdale, D. D., and Beyler, C. L., "An Experimental Evaluation of Critical Temperature as a Criterion for Piloted Ignition," *Fire Safety Journal*, Vol. 13, pp. 185-196, 1988.
- [18] Atreya, A., and Wichman, I. S., "Heat and Mass Transfer During Piloted Ignition of Cellulosic Solids," *Journal of Heat Transfer*, Vol. 111, pp. 719-725, 1989.
- [19] Mohgtaderi, B., Novozhilov, V, Fletcher, D. F., and Kent, J. H., "A New Correlation for Bench-Scale Piloted Ignition Data of Wood," *Fire Safety Journal*, Vol. 29, pp. 41-59, 1997.
- [20] Nelson, M. I., Brindley, J., and McIntosh, A. C., "Ignition Properties of Thermally Thin Materials in the Cone Calorimeter: A Critical Mass Flux Model," *Combustion Science and Technology*, Vols. 113-114, pp. 221-241, 1996.
- [21] Krishnamurthy, R., and Gebhart, B., "An Experimental Study of Transition to Turbulence in Vertical Mixed Convection Flows," *Journal of Heat Transfer*, Vol. 111, pp. 121-130, 1989.
- [22] Jiang, X., and Luo, K. H., "Dynamics and Structure of Transitional Buoyant Jet Diffusion Flames with Side-Wall Effects," *Combustion and Flame*, Vol. 133, pp. 29-45, 2003.

- [23] Bejan, A., *Convection Heat Transfer, Ch. 6*, John Wiley and Sons, New York, pp. 202-223, 1983.
- [24] Kimura, S., and Bejan, A., "Mechanism for Transition to Turbulence in Buoyant Plume Flow," *International Journal of Heat and Mass Transfer*, Vol. 26, pp. 1515-1532, 1983.
- [25] Zukoski, E. E., and Cox, G., *Combustion Fundamentals of Fire, Ch. 3*, Academic, San Diego, 1995.
- [26] Incropera, F. P., and De Witt, D. P., *Fundamentals of Heat and Mass Transfer, Fifth Edition*, John Wiley and Sons, New York, 2002.
- [27] Marshall, A. W., "Effects of Jet Momentum Distribution on Combustion Characteristics in Co-Swirling Flames," Ph.D. Dissertation, University of Maryland, College Park, MD, 1996.
- [28] Kokkala, M., "Heat Transfer to and Ignition of Ceiling by an Impinging Diffusion Flame," *Technical Research Center of Finland, Research Reports*. No. 586, 1989.
- [29] Williamson, J. W. and Marshall, A. W., "Thermal Behavior of Small Fire Plumes," *Proceedings of the Third Joint Meeting of the United States Sections of the Combustion Institute*, Chicago, 2003.
- [30] Quintiere, J. G., "Fundamentals of Fire Phenomena, Draft," University of Maryland, Department of Fire Protection Engineering, College Park, MD, 2003.